博士学位論文

Study of exotic low-temperature ordering of 5f electrons in isostructural heavy-electron compounds URu_2Si_2 and UAu_2Si_2

（重い電子系化合物 URu_2Si_2 および UAu_2Si_2 における 5f 電子低温秩序状態の研究）

田端　千紘

北海道大学大学院理学院
物性物理学専攻

2016年3月

HOKKAIDO UNIVERSITY

DOCTORAL THESIS

Study of exotic low-temperature ordering of 5f electrons in isostructural heavy-electron compounds URu_2Si_2 and UAu_2Si_2

Author:
Chihiro Tabata

Supervisor:
Prof. Dr. Hiroshi Amitsuka
Co-supervisors:
Prof. Dr. Vladimír Sechovský
Prof. Dr. Koji Nemoto
Dr. Tatsuya Yanagisawa
Dr. Yoshihiko Ihara

A thesis submitted in fulfilment of the requirements for the degree of Doctor (Science)

in the

Laboratory of magnetism in strongly-correlated electronic systems
Very low temperature group
Department of Physics

March, 2016

Acknowledgements

I express my gratitude to my committee members, Dr. Yoshihiko Ihara, Dr. Tatsuya Yanagisawa, Prof. Koji Nemoto, Prof. Vladimír Sechovský, and Prof. Hiroshi Amitsuka for helpful discussions, support and encouragement. The experiments on URu_2Si_2 were performed in collaboration with Dr. Toshiya Inami (JAEA, SPring-8), Dr. Shinji Michimura (Saitama University), Dr. Makoto Yokoyama (Ibaraki University). The experiments on UAu_2Si_2 were performed in international collaboration with the members of the group of Prof. Vladimír Sechovský, Dr. Klára Uhlířová and Mr. Michal Vališka (Charles University, Prague, the Czech Republic). Also, the NMR measurements were performed in collaboration with Dr. Yoshihiko Ihara. I thank all of them very warmly for their kind support and patience. In particular, I am deeply grateful to Prof. Vladimír Sechovský for giving me the great opportunity to study in Prague and to obtain the first single crystal of UAu_2Si_2. Over the years, I have benefited from discussions and continuous collaboration with many colleagues and friends in our laboratory of Hokkaido University, from whom I learned so much. I am grateful to Dr. Tatsuya Yanagisawa and Dr. Hiroyuki Hidaka for their helpful discussions and warm encouragement. I would like to thank Mr. Naoyuki Miura for his kind support in Prague and Mr. Shogo Shimmura for his great contribution to the NMR measurements. I am also grateful to Mr. Shota Mombetsu, Mr. Hiraku Saito, Mr. Kenta Uenishi, Mr. Ryoma Nagata, Mr. Taisei Seguchi, Mr. Hiroyuki Inagaki, Ms. Mashiho Takai, Mr. Kota Mizuuchi, Mr. Hiroaki Matsumori, Ms. Eri Tatematsu, Ms. Nana Shikanai, and Mr. Shin Sakai. In particular, I am indebted to Prof. Hiroshi Amitsuka for his extraordinary effort and patience in keeping me motivated to finish my work.

Finally, I thank my family for their patience and warm support, which were necessary ingredients to write this thesis.

Contents

Chapter 1

Introduction

1.1 Strongly correlated electron system

The band theory has achieved a measure of success in explaining most of the fundamental properties related with electrons in solids. It, however, does not provide a good approximation in a situation where the electron-electron Coulomb interactions are sufficiently strong compared with the kinetic energy of the electrons. A system in such a condition is referred to as a "strongly correlated electron system".

Many of intermetallics with d or f electrons are classified into the strongly correlated electron systems, because the intra-atomic Coulomb interactions in the d or f shells may become stronger than their kinetic energy due to weak overlap between the wave functions on neighboring ions and/or weak hybridization with other conduction electrons. Strong electronic correlations give rise to highly unusual electronic and magnetic properties, where many-body effects become relevant and it is hard to predict what emerges in a system upon cooling. Therefore, many materials including transition-metals, rare-earth and actinide elements show various exotic physical properties, which have been attracting many researchers in the condensed matter physics; for example, a large number of studies have been made on high-T_c cuprates, iron-based superconductors, heavy-fermion compounds, and so on.

In the present work, we focus on the heavy-fermion systems with strongly-correlated f electrons. In many compounds including rare-earth or actinide elements, f electrons play the principal role in their low-temperature physical properties. Rare-earth atoms have 4f-incomplete shells and actinide atoms have 5f-ones. Since an f electron has a large azimuthal quantum number of $l = 3$, a large centrifugal potential acts on it, a well-localized electron states with a variety of local degrees of freedom, which suffer quantum fluctuations via a coupling with conduction states.

1.2 Dual nature of 5f electrons

In materials including actinide elements such as U and Np, 5f electrons play a key role in their exhibiting various exotic physical properties as typified by coexistence between magnetism and superconductivity. The 5f-electron systems have been studied intensively for more than 30 years, but not a small part of the nature of electronic and magnetic properties is still veiled, when compared with the 3d and 4f electron systems.

One of the reasons might be simply because the 5f electronic systems have a relatively short history as a research area of magnetism in comparison with the 3d and 4f electron systems. Moreover, the difficulty and complexity of procedures to treat their radioactivity, have made experimental studies time-consuming. Furthermore, there is the essential problem rooted in the nature of 5f electrons themselves; *i. e.*, "how can we describe the dual nature of 5f electrons?"

In general, 3d electrons in metals have well-behaved itinerant character, and we can start from a one-electron band model to treat them theoretically. On the other hand, 4f electrons have strongly localized character as described above, so the picture of localized electrons in a 4f shell can be a good starting point of approximations. In contrast, the localized/itinerant character of 5f electrons lies in between 3d and 4f electrons. Therefore, it is usually quite difficult to set a proper model to approach experimental observations for 5f-electron systems.

Let us take a closer look at this problem of "*itinerant-localized duality of 5f electrons*" by starting with the behavior of 4f electrons in rare-earth compounds. Many of the intermetallics containing light rare-earth elements—Ce, Pr, Nd, and Sm—are basically well explained by considering the one-atomic localized model and adding the c-f hybridization effects as perturbation, through which the localized 4f electrons gradually obtain the itinerant character in the crystal at low temperature below a certain characteristic temperature called Kondo temperature (T_{K}). This ground state with strongly interacting itinerant electrons is so-called the heavy fermion state, where the effective mass of electrons becomes 100 to 1000 times larger than that in normal metals. On the other hand, in many heavy rare-earth intermetallics magnetic phase transitions of localized 4f moments take place, because their inter-site exchange interaction, which also comes from the cf hybridization (RKKY interaction), is more effective than the characteristic energy marked by T_{K}. These itinerant/localized characters of 4f electrons have basically been understood by considering competition between the Kondo effect and the RKKY interaction.

In contrast to the 4f electrons, the 5f electrons behave rather differently. Not a few 5f-electronic intermetallics exhibit both localized and itinerant characters at the same time. That is, coexistence of distinct magnetic order and heavy itinerant electrons is often observed in such compounds. One of the currently hottest topics is a coexistence of ferromagnetic order and superconductivity, which has been found only in uranium compounds such as UCoGe[1], URhGe[2] and UGe_2[3]. This finding has been strongly fascinating many researchers, because the BCS theory tells that magnetic field destroys superconductivity. There have been many other 5f systems keeping attracting our interests because of their exotic physical properties: a non-Fermi-liquid behavior and heavy-fermion superconductivity in UBe_{13}, multiple heavy-fermion superconducting phases in UPt_3 and —this is the object substance of the present work— the hidden order and coexisting superconductivity in URu_2Si_2, and so on. These characteristic properties cannot be fully understood in the framework of the existing theory of magnetism. At the root is the fundamental issue of the itinerant-localized duality of 5f electrons, which is essentially correspondent to the quantum mechanical principle of the waveness and particleness of microscopic objects. Establishment of a comprehensive description of the behavior of 5f electrons in metals will thus be a challenging task, involving development of new pictures and fundamental concepts in solid state physics.

1.3 Uranium 1-2-2 systems

In the 5f-electronic systems, so-called "1-2-2 systems" containing uranium atoms have been investigated since the early period of study on actinide intermetallics. They are often noted as UT_2X_2, with transition-metal atoms at the T-sites and silicon or germanium atoms at the X-sites. For those with silicon atoms at the X-sites, there is a variety of transition-metal elements which can occupy the T-sites; it has been confirmed that

there are thirteen stable compounds which contain each transition metal from Cr to Cu, from Ru to Pd, and from Os to Au in the 3d, 4d, and 5d rows, respectively. This variety can be very useful for a systematic study of the duality of 5f electrons in metals. Interestingly, only 5f electrons of uranium carry magnetic moments in this series of compounds except for the system of Mn. Their crystal structure is $ThCr_2Si_2$ type body-centered tetragonal (space group: No. 139, I4/mmm, D_{4h}^{17}) or $CaBe_2Ge_2$ type simple tetragonal (No. 129, P4/nmm, D_{4h}^{7}) depending on the kind of transition metals at the T-site. These structures are illustrated in Fig. 1.1. Most of the UT_2X_2 compounds except for T = Ir and Pt crystallize in the former type structure, which has only one crystallographic site of uranium atoms. These facts help to simplify a survey of the 5f-electronic properties. Unfortunately, for those with Ge, we have less kinds of compounds, lacking Cr, Ru, Os, and Au systems. In the present work, we focus our attention on the UT_2Si_2 family.

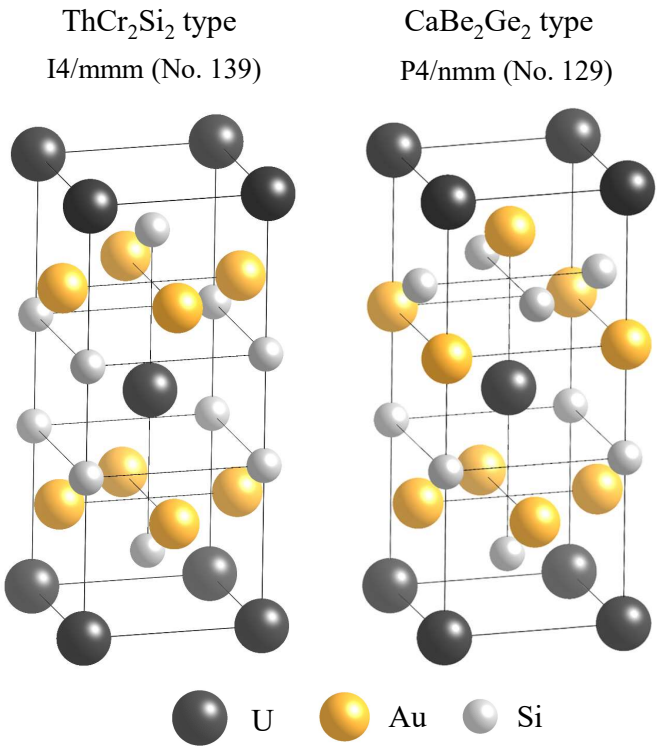

FIGURE 1.1: Two types of crystal structure in which UT_2Si_2 systems crystallize.

1.4 5f-electronic states in UT_2Si_2

The ground state properties in the most UT_2Si_2 systems were investigated in the early studies before 2000s. Their ground states and structural information are listed in Table.1.1. As shown there, magnetic orders take place in many of the systems, for T = Cr, Mn, Co, Ni, Cu, Pd, Rh, Ir, Pt and Au. On the other hand, for the group-8 transition

metals of T = Fe, Ru and Os, no magnetic transition has been observed down to the lowest temperature ever studied.

TABLE 1.1: Crystal-structure data and phase transition temperatures for UT_2Si_2 compounds.

Compound	space group	a (Å)	c (Å)	T_C (K)	T_N (K)	Ref.
UCr_2Si_2	I4/mmm	3.913	10.507	-	27	[4]
UMn_2Si_2	I4/mmm	3.922	10.284	80, 377	-	[5]
UFe_2Si_2	I4/mmm	3.951	9.530	-	-	[5]
UCo_2Si_2	I4/mmm	3.917	9.614	-	85	[6]
UNi_2Si_2	I4/mmm	3.958	9.504	-	124, 103, 53	[6, 7]
UCu_2Si_2	I4/mmm	3.981	9.943	100	106	[6, 8, 9]
URu_2Si_2	I4/mmm	4.128	9.592	-	17.5 (HO)	[10–12]
URh_2Si_2	I4/mmm	4.009	9.771	-	137	[13, 14]
UPd_2Si_2	I4/mmm	4.099	10.070	-	135, 108	[13, 15]
UOs_2Si_2	I4/mmm	4.121	9.681	-	-	[14]
UIr_2Si_2	P4/nmm	4.088	9.790	-	5	[14, 16, 17]
UPt_2Si_2	P4/nmm	4.186	9.630	-	36	[14, 18, 19]
UAu_2Si_2	I4/mmm	4.221	10.258	-	20	[14, 20]

Viewing the magnetic ground states of these UT_2Si_2 systems, we can roughly categorize them into three groups:

(i) Magnetically ordered states where the magnetic moments behave as local moments with the size of $\sim 1\ \mu_B$ per U atom.

(ii) Non-ordering states with moderately enhanced Pauli paramagnetism.

(iii) Heavy-fermion states with reduced magnetic response.

The group (i) consists of the systems with T = Mn, Co, Ni, Cu, Rh, Pd and Pt. The system of Mn is a peculiar case in which not only 5f electrons of U but also 3d electrons of Mn order ferromagnetically at Curie temperatures of ~ 80 K and ~ 377 K, respectively. It is characteristic that others contain group 9, 10, and 11 elements, which have more d-electrons and larger lattice parameters. On the other hand, compounds classified in the group (ii) contain group 8 elements of Fe and Os with less d-electrons and smaller lattice parameters compared with those of the group (i). The remaining members with Cr, Ru, Ir and Au, respectively, would belong to the group (iii). They show different low-temperature properties; UCr_2Si_2 undergoes a structural transition from tetragonal to triclinic (No. 2, $P\bar{1}$, C_i^1) at fairly high temperature of ~ 210 K, and then an antiferromagnetic order at 27 K with an the ordering wave vector of q = (1/2, 1/2, 0). This ordering wave vector is also peculiar, because the other compounds in the group (i) which order antiferromagnetically with ordering vectors along to the tetragonal c-axis. URu_2Si_2 is the most mysterious compound in this family. Although its bulk properties such as specific heat display distinct anomalies that show an evidence of a phase transition occurring at 17.5 K, the order parameter remains a complete puzzle. Details of this compound will be given in the next section. UIr_2Si_2 is a heavy-fermion compound with the largest electronic specific heat coefficient of $\gamma \sim 300$ mJ/K^{2}mol in the UT_2Si_2 family. It orders into a (+-+-) typed AFM structure at around 5 K, where ferromagnetic sheets of magnetic moments pointing in the c-direction stack antiferromagnetically along the

c-axis. This is a common structure in the UT_2Si$_2$ systems; many of the AFM systems in the group (i) order in it. Unlike these, however, UIr$_2$Si$_2$ has rather small magnetically ordered moments of ~ 0.1 $\mu_{\rm B}$ per U atom. UAu$_2$Si$_2$ is seemingly also classified in the group (iii) according to the previous reports. It has been said to order ferromagnetically at 20 K, but the saturation moment is quite small, an order of 0.1 $\mu_{\rm B}$ per U atom. This compound is another object substance of this thesis.

The "*duality of 5f-electrons*" is crucial and the most interesting in understanding these 5f electronic properties in the UT_2Si$_2$ family. For example, in UPd$_2$Si$_2$, a magnetically ordered state is formed by seemingly localized magnetic moments and the transition temperature is much higher than that of many 4f(Ce) compounds. However, curiously enough, moderately enhanced effective mass still remains at the lowest temperature. This means that 5f electrons get involved in both itinerant heavy-fermion and localized-spin components. Some theoretical descriptions have been discussed to explain the behavior of 5f electrons showing this kind of duality in some certain compounds such as UPd$_2$Al$_3$, which is one of the old members of heavy fermion superconductors. However, we have no established theory to fully explain the duality of 5f electrons at present. The present study aims at obtaining some useful information to understand the dual nature of 5f electrons by contributing to the systematic studies of the isostructural 122 uranium compounds.

Chapter 2

Objective

2.1 Desirable missing information in URu_2Si_2 and UAu_2Si_2

In the UT_2Si_2 systems, the electronic ground states of URu_2Si_2 and UAu_2Si_2 are still unclear. For the systematic understanding of electronic properties, it is important to elucidate them and complete the set of information of the UT_2Si_2 systems. In particular, since these two systems show intermediate properties between itinerant and localized characters, they should occupy important places in overview of the dual nature of 5f electrons.

The most enigmatic compound in the UT_2Si_2 systems is URu_2Si_2, which shows a mean-field-like phase transition at 17.5 K without providing any evidences of symmetry breaking [10–12, 21]. This mysterious phase transition has been referred to as "Hidden Order (HO)", keeping attracting many interests since its discovery in middle of 1980s. Furthermore, a fact that superconductivity (SC) appears at $\sim$ 1.5 K makes this compound more interesting. The SC phase exists only in the HO phase; it disappears together with the HO phase by applying pressure above $\sim$ 0.6 GPa [22, 23]. The mechanism of the SC has been also unclear though it is said to have the SC gap of d-wave symmetry [24, 25].

Trying to solve this long-standing mystery of the HO, more than 30 theoretical models have been proposed. However, no model can fully account for the important experimental results accumulated until the present day. It is hopefully expected that elucidating the HO will provide us with a window of opportunity to test how we can understand the 5f electronic state by using these many theoretical models built from various viewpoints of itinerant/localized electronic characters for 5f states.

In contrast to URu_2Si_2, much less reports have been made for UAu_2Si_2. Moreover, it is the last compound in the UT_2Si_2 systems of which a single crystalline sample has never been grown. Five reports on polycrystalline samples have discrepancies about the phase transition, which takes place at 20 K. Lin *et al.* suggest that it is a ferromagnetic order while Rebelsky *et al.* claim that it is a structural phase transition [20, 26]. One of the reasons of this disagreement might be a large sample dependence. Study using single-crystalline samples will provide useful information to clarify low-temperature magnetic properties of this compound.

2.2 Motivation of the present study

The present study was carried out for the primary purpose of elucidating the nature of the phase transitions of URu_2Si_2 (17.5 K) and UAu_2Si_2 (20 K) for a discussion of dual nature of 5f electrons in the UT_2Si_2 systems. In order to achieve this purpose, we considered that the following studies must be crucial for each compound.

- URu_2Si_2: Careful investigation of the symmetry lowering below the transition temperature is necessary. In the present study, we focused on the four-fold rotational symmetry of the crystal structure.
- UAu_2Si_2: First, the single-crystalline growth and investigation of its physical properties at low temperature are necessary. Microscopic experiments are also necessary to elucidate the magnetic structure.

Chapter 3

Study on four-fold rotational symmetry of crystal structure of URu_2Si_2

3.1 Introduction

Nature of the so-called “Hidden Order (HO)"of URu_2Si_2 has been a long-standing mystery in the heavy-fermion physics [10–12, 21]. Despite a clear evidence of a second-order phase transition seen in specific heat and other bulk quantities at the ordering temperature, 17.5 K ($\equiv T_o$), no clear superlattice reflection that may reveal an order parameter has been detected in neutron-diffraction [27–30] and X-ray-diffraction (XRD) [31–34] measurements. Due to the lack of experimental evidence for conventional spin-density-wave and charge-density-wave ordering, a variety of exotic order parameters have been proposed in different theoretical approaches, generating vigorous debate on fundamental issues of possible ground states in strongly correlated f-electron materials [35, 36].

Recently, broken four-fold rotational symmetry about the tetragonal c axis in HO was suggested on the basis of measurements of magnetic-torque [37, 38], cyclotron-resonance [39, 40], ^{29}Si-NMR [41], XRD [42], and elasto-resistance [43]. The former three experiments demonstrate that the symmetry of an electron system is lowered, while the latter two exhibit that a crystal-lattice distortion is coupled with the electron ordering. The electron order is considered to be uniform and orientational, and thus called “nematic". The ordered domains were estimated to be approximately 40 μm in length, from the magnetic-torque measurements [37]. These findings are expected to provide a crucial key to solve the issue of HO, because the broken rotational symmetry imposes strong constraints on existing and planned theoretical considerations [35, 36].

Among various observations, we would like to focus our attention onto the spontaneous lattice deformation observed in the recent XRD measurements [42], because a lattice parameter is a fundamental thermodynamic quantity observable in zero magnetic field and may provide a direct and definitive evidence. Tonegawa and his colleagues investigated the symmetry of two URu_2Si_2 single crystals, which are distinguished by their contrastive values of residual resistivity ratio (RRR): one has a low RRR of ~ 10 and another has a very high RRR of ~ 670 [42]. A tetragonal-to-orthorhombic deformation was found only in the latter high-RRR sample. The magnitude of distortion, measured by the “orthorhombicity (ϵ)", is reported to be $\epsilon \sim 8 \times 10^{-5}$ just below T_o. Here, the orthorhombicity is defined as

$$\epsilon \equiv \frac{|b' - a'|}{b' + a'} = \frac{|d_{110} - d_{1\bar{1}0}|}{d_{110} + d_{1\bar{1}0}}, \tag{3.1}$$

where a' and b' are newly defined orthorhombic lattice parameters, and d_{hkl} denotes the interplanar spacing for the initial tetragonal indices hkl. They also pointed out that the nematicity appears via a sharp first-order phase transition.

They argue that the presence or absence of the lattice distortion is ascribed to the difference in RRR, and suggest that an inherent electron-lattice coupling in a shear mode is depressed by impurities in the low-RRR sample. On the other hand, it is known that major thermodynamic characteristics of HO including thermal expansion is almost independent of the sample quality [44–46]. The linear-thermal-expansion coefficients measured along [100] and [010] or [110] and [1$\bar{1}$0] are known to superpose to each other within the accuracy of $\sim 1 \times 10^{-7}$ [47, 48]. In addition, ultrasonic investigations of elastic constants reveal the presence of weak but detectable electron-lattice coupling in all the modes including the shear $c_{66}(xy)$ mode; however, to date, no signal that may indicate a uniform lattice distortion has ever been detected [48–54]. At present, it may not be obvious how the lattice distortion of $\epsilon \sim \mathcal{O}(10^{-4})$ decreases or cancels out to within the detective limit of capacitance dilatometry and gives no influence to the ultrasonic detection of elastic constants, depending on the magnitude of RRR. Therefore, it will be worthwhile to test the reproducibility of the lattice distortion by using a different single crystal and different experimental setup for better understanding of the nature of nematic behavior. In this paper, we present our latest XRD study on URu_2Si_2 with the highest instrumental resolution ever used on this compound.

3.2 Experimental Procedure

A single crystal of URu_2Si_2 (RRR $\sim$ 20) was grown by the Czochralski method and vacuum-annealed at 1000 °C for one week. The crystal was then carefully crushed into small pieces by using an agate mortar and pestle. Mosaicity of several pieces was checked by observing Bragg spots at high diffraction angles with a Rigaku DSC imaging plate diffractometer and Si(111) monochromatized synchrotron radiation X-rays ($\lambda = 0.729$ Å) at the BL-8B beamline of the Photon Factory, KEK. A crystal piece which has the smallest mosaicity showing no distortion of the spots was selected and oriented for higher resolution experiments at SPring-8. The size of this piece is approximately $30 \times 30 \times 30 \mu\mathrm{m}^3$. Note that, at this stage, the crystallographic quality was checked only in the resolution of the imaging plate: $\Delta d/d \sim 7.0 \times 10^{-4}$ (FWHM).

The high-resolution XRD measurements were performed using synchrotron X-ray at the beamline BL22XU, SPring-8. The incident X-ray energy was chosen to be 10.6254 keV ($\lambda = 1.16607$ Å) to observe a (550) Bragg peak in a backscattering geometry. The corresponding X-ray attenuation length is approximately 8.7 μm. The sample was glued on a thin copper needle with GE-7031 varnish, and cooled down to $\sim$ 5 K in a standard ILL ^{4}He gas-flow “orange" cryostat. Figure 3.1 shows a schematic view of the experimental setup. The cryostat was installed on a two-axis goniometer to optimize an alignment of crystal axes by tuning two angles ω and χ on horizontal and vertical planes, respectively. The incident X-ray beam was monochromated by using a standard Si(111) monochromator followed by a high-resolution Si(660) monochromator (HRM). A backscattering configuration was constructed by placing a photodiode detector at a distance of 4.49 m away from the sample and $\sim$ 15 mm from the optical axis of the incident beam. Consequently, the diffraction angle 2θ reaches 179.81° in this setup. A 1.0 mm ϕ pinhole placed in front of the detector window provides an accuracy of the diffraction angle: $\Delta\theta \sim 0.013^\circ$. A successful observation of a tiny distortion

evidencing hidden magnetic-octupole order in $Ce_{0.7}La_{0.3}B_6$ was recently achieved by Inami *et al.* by using this experimental setup [55].

The instrumental resolution for an interplanar spacing d is derived from the Bragg's law as follows:

$$\frac{\Delta d}{d} = \sqrt{\left|\frac{\Delta\lambda}{\lambda}\right|^2 + |\cot\theta\Delta\theta|^2}. \tag{3.2}$$

The first term in the square root is given by the accuracy of the monochromator. The HRM in the present measurements ensures $\Delta\lambda/\lambda \sim 7.2 \times 10^{-6}$ (FWHM). On the other hand, the second term yields $\cot\theta\Delta\theta \sim 8.0 \times 10^{-7}$, which is one order smaller than the first term. The instrumental spatial resolution of the present setup is thus given as $\Delta d/d \sim 7.3 \times 10^{-6}$ (FWHM), which is roughly four times higher than the previous report[42]. Hereafter we call the measurements with HRM a "high-resolution mode" and those without HRM a "normal-resolution mode". The spatial resolution in the latter is estimated to be $\sim 1.0 \times 10^{-4}$.

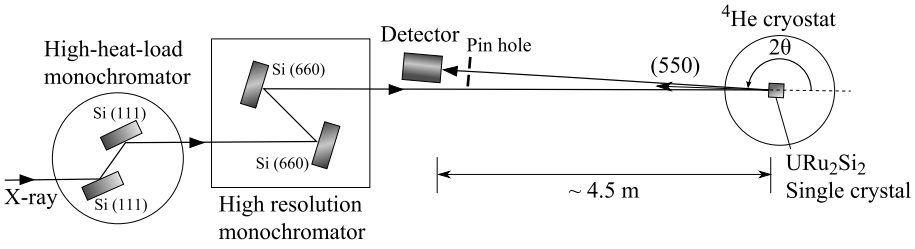

FIGURE 3.1: Schematic view of the experimental set-up.

Radial (longitudinal) scans in the present experiments were carried out by changing an energy of the incident beam, instead of the usual θ-2θ scans (see Figure 3.2). This method provides a notable advantage on keeping the scanning position on the same line precisely, because it is not necessary to move a detector and a sample during a scan.

3.3 Results

Figure 3.3 exemplifies the results of ω scans (rocking curves) and χ scans, which were performed to check the crystal mosaicity and optimize a sample tilt before each radial scan. All the observed profiles exhibit an extremely narrow FWHM ($\sim 0.02^\circ$), indicating that the crystal we used has very low mosaicity. There is a weak asymmetry in the rocking curves, which indicates the presence of inhomogeneous distributions of misorientation angles in this sample. We did not find any significant change in the peak shape upon cooling.

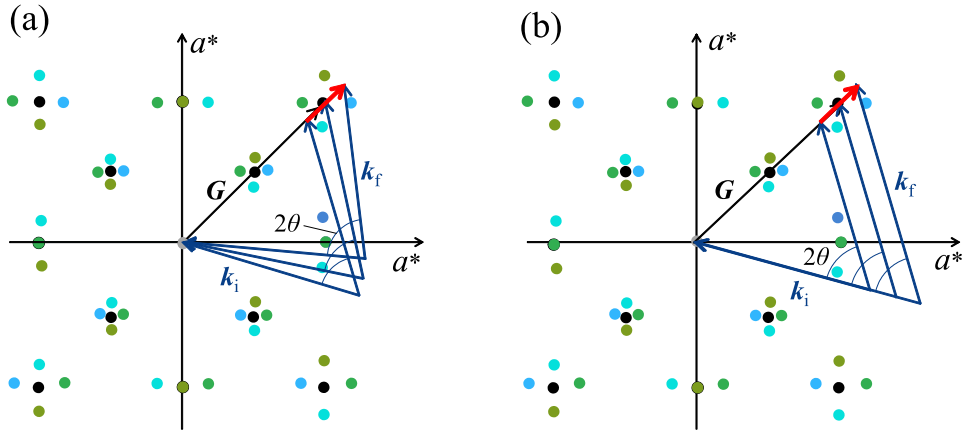

FIGURE 3.2: Schematic view of two different radial-scan methods: (a) a usual $\theta - 2\theta$ scan and (b) a scan by tuning wavelength. Black and color dots in backgrounds indicate the reciprocal lattice points in the basal planes of tetragonal and orthorhombic structures, respectively: Four different colors correspond to four domains.

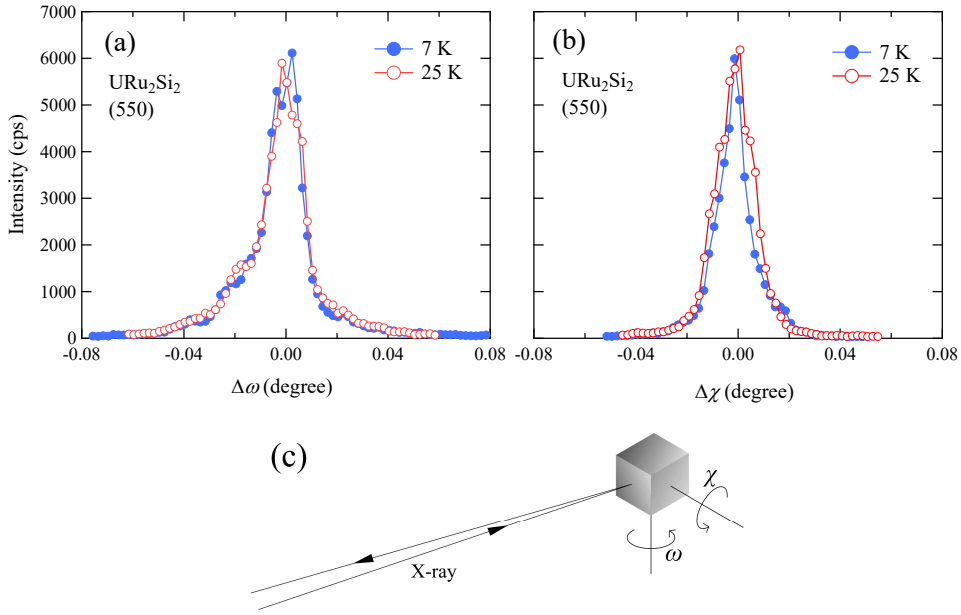

FIGURE 3.3: Experimental results of (a) ω scan and (b) χ scan of URu_2Si_2at 7 and 25 K, and (c) schematic view of the definition of two orthogonal tilt angles.

Figure 3.4 displays the (550) Bragg-peak profiles obtained from the radial scans, which were performed with and without HRM in the temperature range between 5 and 30 K. We found that the peak shapes observed in the high-resolution mode are clearly distorted over the whole temperature range, in contrast to those in the normal-resolution mode. This remarkable difference was led by the improvement of resolution that has enabled us to observe a fine structure of the peak profile. Considering the

narrow widths of the ω-scan and χ-scan profiles (Figure 3.3), we can ascribe the fine structure seen in the radial scans to a distribution of lattice parameters rather than an effect of anisotropy in a resolution function. Regarding the temperature variations, we did not find any signature of broadening and splitting of the (550) peak. On the other hand, the peak position shifts toward higher energies as temperature is lowered, indicating that the (110) interplanar spacing d_s shrinks significantly upon cooling.

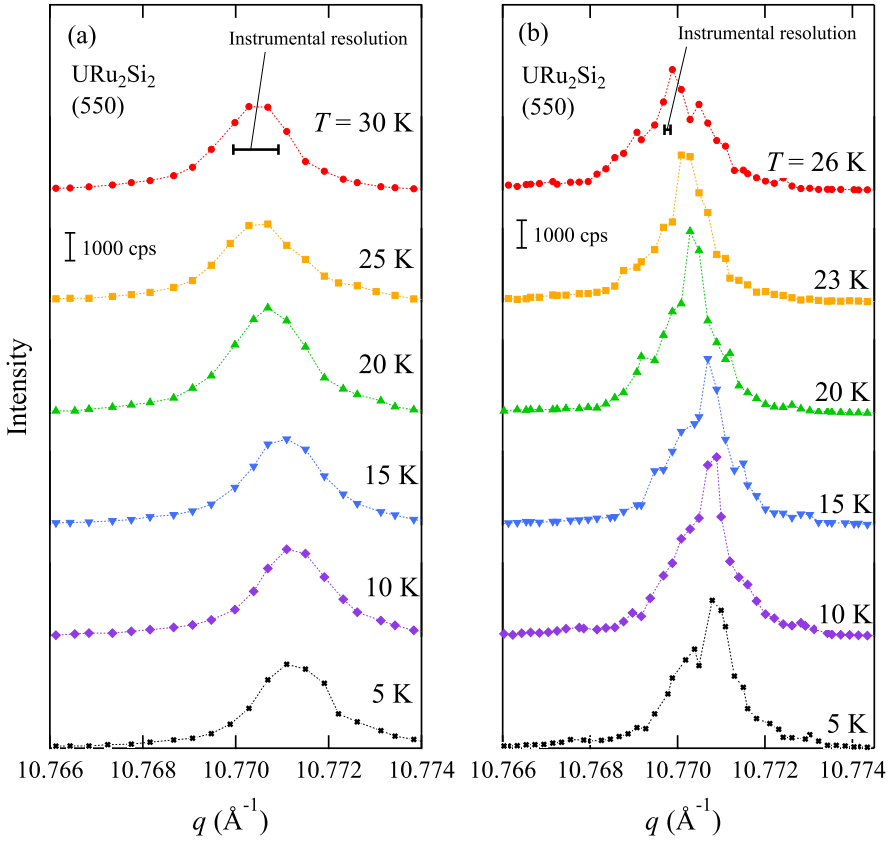

FIGURE 3.4: Examples of the (5 5 0) peak profiles of URu_2Si_2measured in (a) the normal-resolution mode and (b) the high-resolution mode.

We fit the observed (550) Bragg peaks with a Lorentzian function to evaluate the mean and the FWHM. The FWHM is then converted to the deviation of d_s with the instrumental resolution being considered. The mean, $\bar{d}_s$, should be proportional to the a-axis lattice parameter if the crystal stays in the same tetragonal structure. In Figure 3.5 (a), we plotted temperature dependence of a relative change in $\bar{d}_s$, compared with the a values, which are extracted from the previous studies of a linear thermal-expansion coefficient [47] and neutron Larmor diffraction [56, 57]. It can be seen that they are in good quantitative agreement, including a small kink anomaly at T_o. (We carefully checked by changing incident-beam intensity that the X-ray radiation did not heat up the sample.) Figure 3.5 (b) displays the relative deviation, $\Delta d_s/d_s$ (FWHM), versus temperature. The analyses for the two resolution modes yield approximately the same value: $\Delta d_s/d_s \sim 1.2 \times 10^{-4}$, which shows no significant temperature variation. Note that if the same distortion reported in the previous work [42] took place in our case,

$\Delta d_{\rm s}/d_{\rm s}$ should be doubled in magnitude below $T_{\rm o}$.

The xy-type orthorhombic distortion, which is currently being debated, usually forms a twin structure resulting in broadening or splitting of the tetragonal Bragg spots (see Figure 3.2). We have estimated an allowable magnitude of the crystal distortion in our observation by using the standard deviation σ of the peak fitting, which is indicated by error bars in Figure 3.5 (b). The σ can be interpreted as 68 percent confidence interval if the measured values are normally-distributed with a mean value $\overline{w}$ (i.e., the true value w is included in an interval $\overline{w}\pm\sigma$ with probability 0.68). Within this statistical significance, we conclude that the orthorhombic distortion with ϵ exceeding $\sim 3\times10^{-5}$ is not present in this URu_2Si_2 single crystal.

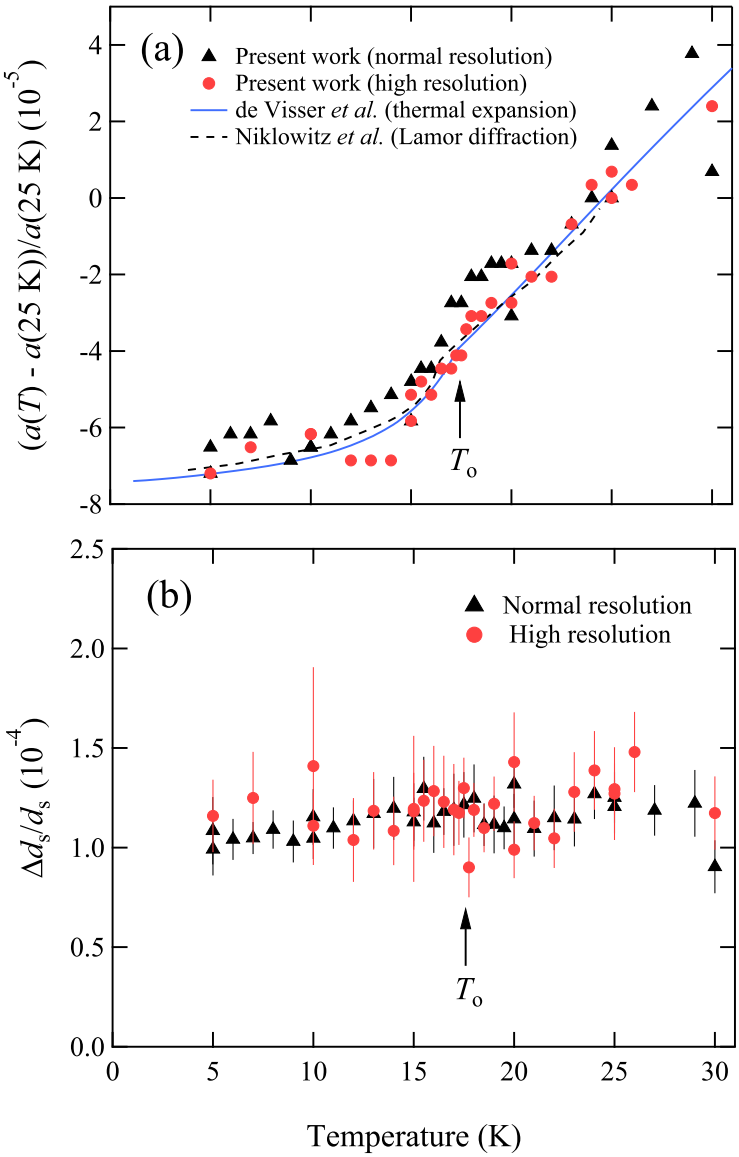

FIGURE 3.5: Parameters obtained from the fitting of the (5 5 0) radial-scan profiles of URu_2Si_2. (a) Temperature dependence of the relative change in the (1 1 0) interplanar spacing and the a-axis lattice parameters extracted from the previous studies of thermal-expansion[47] and neutron Larmor diffraction[56, 57]. (b) Temperature dependence of the relative deviation of the (1 1 0) interplanar spacing. The error bars indicate the standard deviation σ of the fitting. The data points in the high-resolution mode are scattered more widely than those in the low-resolution mode. This is due to a worse-fit convergence caused by a fine structure observed in the high-resolution peak profiles.

TABLE 3.1: Mean values of lattice parameters $\bar{a}$ and coherence lengths evaluated from the three Lorentzian fits described in Fig.3.6.

Fitting curves	$\bar{a}$ (Å)	Coherence length (Å)
f_1	4.1251	6.3×10^3
f_2	4.1248	1.4×10^4
f_3	4.1247	5.0×10^3

3.4 Discussions

3.4.1 Distribution of the lattice constants

Now we discuss the fine structure of the peak profiles observed in high-resolution mode. The distorted shape of the peaks suggests that the present sample is composed of several “crystallites" with discrete averages in lattice parameter. We have found that the observed peak profiles can fairly well be described by the sum of three Lorentzian functions f_1, f_2 and f_3 at least, as shown in Figure 3.6. The narrowest component f_2 shows the FWHM of $\sim 4.5 \times 10^{-5}$ Å^{-1}, which corresponds to $\Delta d_s/d_s \sim 2.9 \times 10^{-5}$ and a coherence length of $\sim 1.4\mu$m. The mean value of a and the coherence length estimated for each crystallite are summarized in Table 3.1. The inherent distribution of the lattice parameters in URu_2Si_2 was first predicted by neutron-diffraction studies under uniaxial stress [58, 59], and then confirmed by neutron-Larmor-diffraction measurements [56, 57, 60]. Through those studies together with NMR [61] and μSR [62], it is now widely accepted that weak antiferromagnetism at ambient pressure is a phase separation phenomenon induced by residual stress, which is distributed in a crystal. The relative distribution widths, $\Delta a/a$, estimated by the neutron-Larmor-diffraction studies are $\sim 4.05 \times 10^{-4}$ [56, 57] and $\sim 4.5 \times 10^{-4}$ [60], roughly four times larger than the present result, $\Delta a/a \sim 1.2 \times 10^{-4}$. This difference is probably due to a large difference in the size of used crystals. The outcome of the present study is that the distribution of lattice parameters of this compound can become nonuniform in the length scale of the order of 10^{-4} Å. The observed multipeak structure of the lattice-parameter distribution might be consistent with a prediction given by the recent study on the sample-quality effects [45]. We would like to reemphasize in Figure 3.6 that there is no significant difference in the peak profile between 5 K and 30 K, even when focusing on the fine structure.

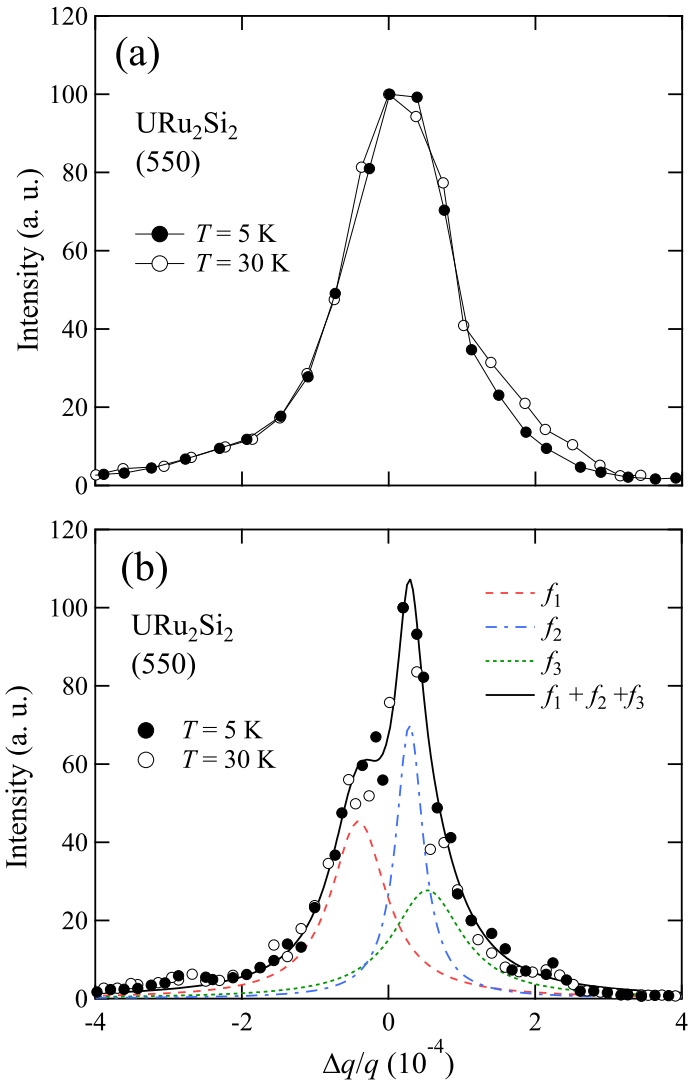

FIGURE 3.6: The (5 5 0) peak profiles of URu_2Si_2measured in (a) normal resolution mode and (b) high-resolution mode at 5 and 30 K. Broken and solid curves represent the best fit of the high-resolution profile with a sum of three Lorentzians.

3.4.2 Sample quality and the HO

The fact that the structural change is not observed in our study might be due to the low quality of our sample (RRR $\sim$ 20), as argued by Tonegawa *et al.* [42]. However, the ^{29}Si-NMR measurements using the same lot of our sample have revealed a sharp emergence of internal fields along the basal plane [63]. Although the magnitude of the internal fields is very weak, this behavior might be regarded as a sign of the nematic order [42]. It is therefore considered that the nematic behavior itself is essentially independent of RRR, no matter if the behavior is intrinsic or extrinsic to HO. In consequence, whether or not the lattice distortion is induced by HO might be ascribed to the effects of RRR on the magnitude of electron-lattice coupling, as they proposed [42]. In this context, it is suggested that the impurities might strongly suppress the electron-lattice couplings in shear modes, so that the lattice does not feel the symmetry breaking fields.

3.4.3 Electron-lattice coupling in URu_2Si_2

On the other hand, robust characteristics of HO are sharp and mean-field-like anomalies observed at T_o in various thermodynamic quantities such as specific heat, thermal expansion, magnetic susceptibility, etc., which should be related to each other via thermodynamic relationships. It is empirically known that in URu_2Si_2 these quantities follow the similar temperature dependence when displayed as $C_{5f}(T)$, $\alpha_V(T)$, and $d(T\chi_c(T))/dT$, where C_{5f} denotes the 5f-electronic contribution to the specific heat [64], α_V the volume thermal-expansion coefficient [47], and χ_c the c-axis magnetic susceptibility [64] (Figure 3.7). The proportionality between α_V and C_{5f} implies the presence of a Grüneisen parameter, which describes the volume dependence of characteristic energy scales associated with the low-temperature states including HO [65, 66]. On the other hand, the proportionality between C_{5f} and $d(T\chi_c)/dT$ is known as Fisher's relation, which was originally discussed in antiferromagnetic systems [67, 68]. What should be noted here is that the presence of the Grüneisen parameter ensures the presence of a finite electron-lattice coupling in the symmetry conservative modes. The direct evidence has indeed been obtained by the measurements of elastic constants [50, 54]. These features have been established in a standard (low-RRR) sample, but are expected to be dramatically modified in a high-RRR sample because of a large orthorhombic distortion together with a switching of the nature of phase transition between second and first order, if the above scenario of the nematic order is true. It will also be of particular interest to investigate how only a shear-mode electron-lattice coupling can significantly be enhanced with RRR.

3.4.4 Remaining candidates for the HO

We have confirmed that the structural 4-fold rotational symmetry is hold in the HO phase in our sample within the high experimental accuracy. Then what kind of the symmetry breaking is left for the HO? In the early times, antiferromagnetic order of largely reduced moments had been believed to be the nature of the HO[69–73]. However, from the detection of the existence of a small amount of the phase-separated AFM phase, possibility of other kind of order parameters have been discussed. Particularly, the order of higher-rank multipoles have been a strong candidate for the HO, because of no detectable unambiguous emergence of internal magnetic fields accompanied by the HO. Here we examine some major candidates and experimental investigation of them done till today.

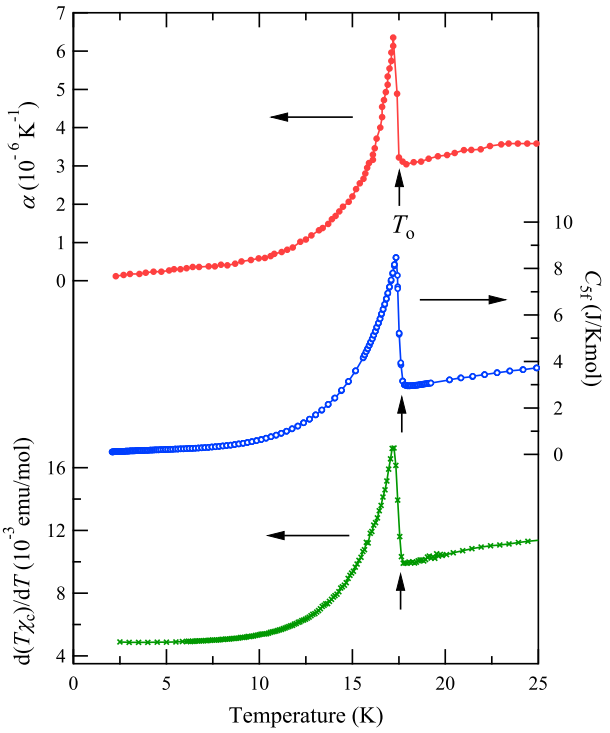

FIGURE 3.7: Temperature variations of 5f-electronic specific heat C_{5f}[64], linear thermal-expansion coefficient α_V[47] and a temperature derivative of c-axis susceptibility χ_c multiplied by temperature[64].

Electric quadrupole order

Electric quadrupole is a rank-2 multipole. The most models have been proposed about the electric quadrupole order[74–80]. They take a stance where the HO does not violate the time-reversal symmetry. Many of the models are of the antiferro quadrupole(AFQ) order which break the translational symmetry. In order to investigate the possibility of the AFQ order, resonant X-ray scattering (RXS) experiments have been performed by Amitsuka $etal.$, but no detectable signal which indicates the AFQ order in the HO state was observed[33]. Although the RXS experiments did not eliminate ferroquadrupole models, it is basically incompatible with the present results and facts that the corresponding mode of the elastic constants does not show softening large enough to account for them.

Magnetic octupole/dotriacontapole order

The magnetic octupole(rank-3)[81, 82] and dotriacontapole(rank-5)[83] models have been also considered. If they really take place as the HO state, the time-reversal symmetry should be broken. That is, they take a stance to regard the extremely tiny but finite internal field of < 0.5 G observed in ^{29}Si-NMR experiments as an intrinsic property in the HO[63]. However, no valid evidence has been obtained from the neutron or X-ray diffraction experiments, that is, no superlattice reflection has been ever observed.

Electric hexadecapole order

The antiferro-hexadecapole(AFH) order was predicted by Haule and Kotliar in 2009. Few years later an AFH ordering model has been constructed by Kusunose $etal.$ in 2011 based on localized f-electron picture[84]. Shortly after it, our group performed RXS experiments to examine it by searching the signal from the quadrupole which should be induced by applying magnetic field in a certain direction. As a result, no signal indicating that the proposed order took place was detected in the experimental accuracy. However, since there was a malfunction of the experimental instruments at that moment, we could have a chance to investigate the possibility of the AFH in higher level of accuracy.

Another possibility

Then what candidate is left for us if the possibilities of the multipolar ordering were all eliminated? Although we have been searching a superlattice reflection that is critical to identify the HO, we have never found it before. This fact may let us think that the superlattice reflection does *not* exist intrinsically, namely indicating that no translational symmetry is broken, which means the order of $\boldsymbol{q} = 0$. Not only the translational symmetry, but also even the other kinds of symmetry can be hold if we get out of the idea that the HO is the second-ordered phase transition. In other words, let us think that, "what if the HO is a first-ordered phase transition?". The HO has been considered to be the second-ordered one because of the shape of the specific heat anomaly at $T_{\rm o}$. However, there is still a certain possibility of a weak first-order phase transition which is difficult to distinguish from a second-order one. If the HO is first order, there should be no order parameter which is zero in the high temperature phase and has a finite value only in the ordered phase. In order to investigate it, the following experiments may be useful:

- Differential thermal analyses to test whether latent heat is released or not.
- RXS or neutron diffraction experiments for a careful investigation of the basic reflection intensities to detect the signal due to uniformly ordered components.

3.5 Conclusions

We studied the crystal-lattice symmetry of URu_2Si_2 by means of synchrotron X-ray diffraction with the highest instrumental resolution ever applied for this compound. We confirmed that a “standard" sample with RRR $\sim$20 shows no signature of the tetragonal-to-orthorhombic distortion within the experimental accuracy of the orthorhombicity: $\epsilon = |b' - a'|/(b' + a') < 3 \times 10^{-5}$, where the “standard" means that the sample exhibits major dynamic and thermodynamic characteristics associate with HO. Using the high spatial resolution setup, we further revealed that the distribution of lattice parameters is “nonuniform", suggesting that the sample is composed of several crystal grains in the sizes of $\sim 1\mu$m and with lattice parameters spread in the range $\Delta a/a < 1.2 \times 10^{-4}$. We should note that a URu_2Si_2 sample is inherently inhomogeneous in the crystal structure to this extent, by which we know at least fragmentary antiferromagnetic order can be induced. Further studies to characterize the relationship between crystallographic conditions and electronic properties of this system is clearly needed.

Chapter 4

Low-temperature magnetism of UAu_2Si_2

4.1 Previous report on UAu_2Si_2

UAu_2Si_2 is the least investigated UT_2X_2 compound. There have been only five reports about this compound since its discovery in 1986 by Palstra et al. until the latest one in 1997 given by Lin et al. [14, 20, 26, 85, 86]. All of them are about studies of polycrystalline samples, that is, no report of single crystal growth has been ever given. According to most of the previous reports, UAu_2Si_2 crystallizes in the $ThCr_2Si_2$ type body-centered tetragonal (I4/mmm) structure as is the case of the most other UT_2X_2 compounds. However, only Palstra et al. suggested the $CaBe_2Ge_2$ type simple tetragonal (P4/nmm), which is another type of structure in which the UPr_2X_2 and UIr_2X_2 compounds crystallize. As one of the most characteristic properties of UAu_2Si_2, it has shown large sample dependences in its physical quantities, which makes things more complicated. Lin *et al.* investigated the annealing effects on this compound and pointed out differences in annealing conditions as the reason of the sample dependences. In their reports, as-cast samples show two ferromagnetic (FM) like anomalies in magnetization at about 82 K and 20 K. On the other hand, well annealed samples do not show any anomaly around 82 K in physical properties such as magnetization, specific heat and electrical resistivity. Instead, they show another FM like anomaly at around 50 K and then, an anomaly similar to that in as-cast samples at 20 K follows. The authors of the reports have made different speculations for the each FM-like anomalies; canted antiferromagnetic and spiral magnetic order for the anomaly around 82 K, a structural transition and spin flip transition for that around 50 K. They seem to almost reach consensus on the origin of the anomaly around 20 K, concluding that it is a FM order, although only Rebelsky et al. claimed that it was a structural transition by means of powder X-ray and neutron diffraction [26].

Only the 20 K anomaly has been confirmed as a second-order phase transition by a specific heat measurement by Lin [20]. Now we define the transition temperature as $T_{\rm m}$. Even in this possibly FM ordered phase below $T_{\rm m}$, relatively large electronic specific coefficient of $\gamma \sim 100$ mJ/K^{2}mol still remains. Moreover, the saturating ordered moment is quite small, $\mu_{\rm sat}{\sim}0.07\mu_{\rm B}$ per uranium ion. These might be an indication of existence of itinerant 5f electron at low temperature. Some uranium intermetallic compounds such as UGe_2 [3, 87], URhGe [2] and UCoGe [1, 88], which show the heavy-fermion behavior of itinerant 5f electrons with FM ordered state, exhibit unconventional superconducting phases. UAu_2Si_2 may also have potential to have such an exotic property.

TABLE 4.1: Structural parameters (lattice constants and the atomic position of Si atoms) of annealed UAu_2Si_2 obtained by the Reitveld analyses using a software RIETAN-FP. The typical reliability factors are $R_{\rm wp} = 12\%$, $R_{\rm F} = 3.8\%$, $S = 1.8$.

T (K)	a (Å)	c (Å)	$z_{\rm Si}$
293	4.223(1)	10.290(1)	0.391(1)
8	4.207(1)	10.280(1)	0.390(1)

4.2 Purposes

In the present work, we succeeded in growing single crystals of UAu_2Si_2, for the first time. In order to reveal the structural, thermal, magnetic, and transport properties of this compound, we performed powder X-ray diffraction (XRD), measurements of specific heat, magnetization, and electrical resistivity in the temperature range of ∼2 K to ∼300 K.

4.3 Experimental procedure

Firstly, polycrystalline samples of UAu_2Si_2 were synthesized by arc-melting in Ar atmosphere, with stoichiometric amount of the starting materials of U(99.9%), Au(99.99%) and Si(99.999%) in Sapporo. Powder X-ray diffraction patterns of the as-cast samples have some peaks which cannot be explained by either the $ThCr_2Si_2$ typed structure or the $CaBe_2Ge_2$ typed one. Intensities of the unidentified peaks are ∼10 % of a main peak of UAu_2Si_2, which is too large when considering contributions of impurities, so those peaks should come from some binary phases — composed of some compounds with different chemical compositions from that of 1-2-2. These peaks of the binary phases have almost the same position of the diffraction angle as reported by Lin describing them as "unidentified peaks" [20]. After annealing in vacuum at a temperature of 900°C for 2 weeks, the unidentified peaks all vanished from XRD patterns, and all remained peaks were explained by the $ThCr_2Si_2$ type body-centered tetragonal structure. No change was observed in the diffraction patterns measured at 293 K and 8 K. The refined lattice parameters are listed in the Table 4.1. We also prepared polycrystalline $ThAu_2Si_2$ samples in the same manner as above, and observed similar annealing effects.

Next we tried to grow single crystals of UAu_2Si_2 by floating zone melting method using an optical furnace in Department of condensed matter physics, Charles University, Prague. The purity of starting materials are U(99.9%), Au(99.99%) and Si(99.999%). The melted rod itself was, unfortunately, not single crystalline like but composed of many macroscopic crystallites of single crystal which have different orientations from each other. The size of the crystallites were about 1 mm at a maximum, which made us enable to dig out a few pieces of the crystallites. For the obtained crystallites, a tetragonal structure with the lattice constants $a = 4.213, c = 10.31$ was confirmed by single crystal XRD and 4-fold rotational symmetric Laue patterns were observed. No superconductivity was observed down to ∼ 65 mK in resistivity measurements.

Magnetization was measured by a SQUID magnetometer of MPMS provided by Quantum Design Inc. in the temperature range from 2 to 300 K. Specific heat was measured by the thermal relaxation technique in the temperature range from 5 to 200 K in the magnetic fields up to 9 T by a PPMS, also provided by Quantum Design Inc. Electrical resistivity was measured by the conventional four-probe method in the temperature range from 2 to 350 K in the magnetic fields of 0 T and 9 T by using the PPMS.

In order to get microscopic information, we also performed ^{29}Si-NMR measurements on the polycrystalline sample grown in Hokkaido University. After annealing at 900°C for 7 days, the sample was crushed into powder and mixed with stycast 1266. Then it was solidified in magnetic field of ~ 1 T so that the powdered sample became fixed in a magnetically oriented alignment. The field-sweep NMR spectra were taken by the spin-echo method. We chose a frequency of 38.5 MHz for the measurements. The external field was calibrated from ^{63}Cu resonance. The temperature range studied was from 80 K down to 4.2 K.

4.4 Results

4.4.1 Specific heat

Figure 4.1 shows the temperature dependence of the specific heat. A distinct lambda anomaly was observed at T_m = 19 K, indicating an occurrence of second-order phase transition. The phase transition is due to 5f electrons of uranium ions, because no anomaly was observed in the specific heat of polycrystalline $ThAu_2Si_2$ with no 5f electron. The electronic specific-heat coefficient is significantly large; $\gamma \sim 150\ \mathrm{mJ/K^2mol}$.

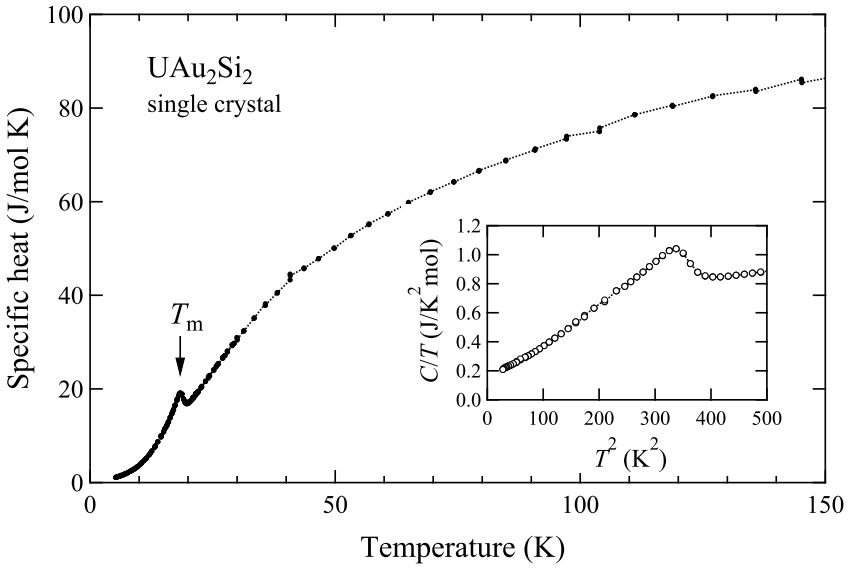

FIGURE 4.1: Temperature dependence of the specific heat of single-crystalline UAu_2Si_2. The inset shows low-temperature-specific heat, C, divided by temperature, as a function of T^2.

In magnetic fields, the specific heat around T_m behaves rather differently depending on a direction of the applied field as shown in Fig. 4.2. Its temperature dependence shows a more pronounced peak anomaly at T_m by increasing the field along [001]; the peak becomes sharper and larger, meaning that the more entropy is released due to the phase transition, which is considerably different, from the behavior that is expected for usual ferromagnetic systems, where a specific-heat peak associated with the FM transition becomes broader by applying magnetic fields. In contrast, it does not show any significant change by applying the field along [100]. This result suggests that the order below T_m is more stabilized by applying magnetic field only along the [001] axis. The γ value is reduced by increasing the fields along [001]; it decreases about 20 percent in the field of 9 T, corresponding to the enhancement of the entropy release at the transition temperature by applying the fields.

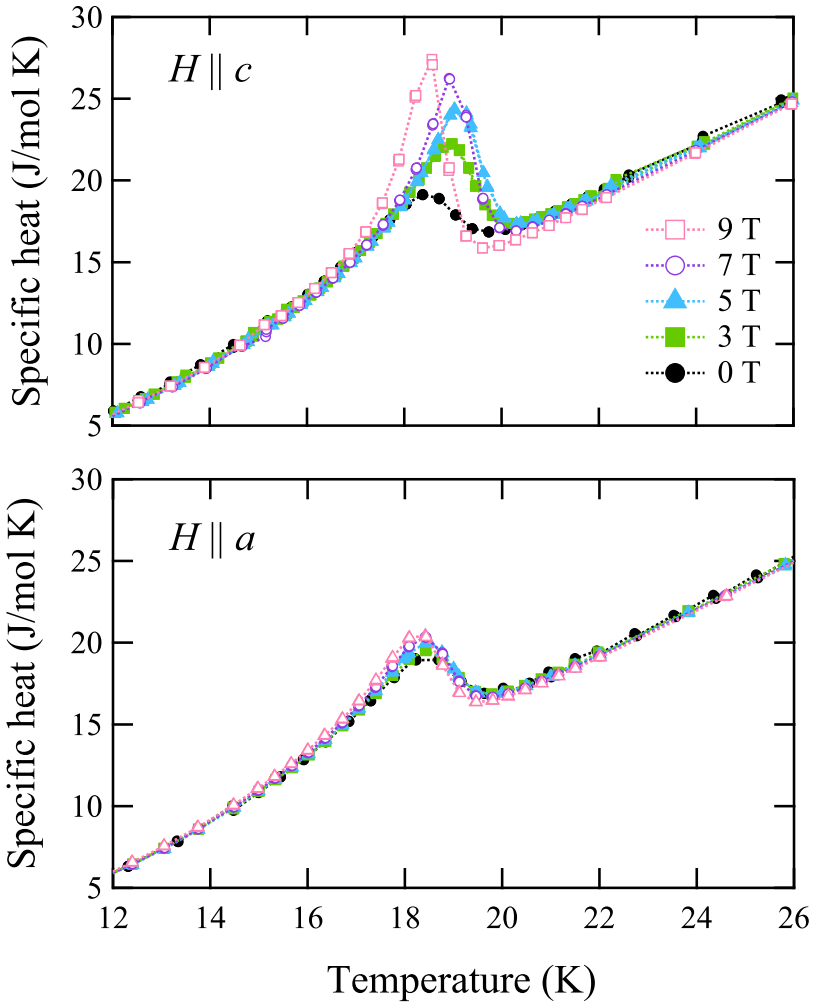

FIGURE 4.2: Temperature dependence of the specific heat of single crystal UAu_2Si_2 measured in magnetic fields along two crystallographic axes, [001] (upper) and [100] (bottom).

4.4.2 Electrical resistivity

The temperature dependence of electrical resistivity is shown in Fig. 4.3. The observed behaviors are far from the typical metallic ones; the resistivity increases with decreasing temperature for both the crystallographic axes of [100] and [001]. The increase of the resistivity is suppressed around 40 K, suggesting that the scattering becomes coherent at the lower temperature. A dip-like anomaly appears at 34 K in the both current directions. It is not clear whether it is the bulk property of the sample or not, because no anomaly has been observed in the specific heat at this temperature and it has never been observed in either polycrystalline samples which we synthesized in Sapporo nor those used in the previous studies. By applying longitudinal magnetic field of 9 T, the dip-like anomaly disappears and it seems that the suppression of the resistivity by the magnetic field becomes pronounced below this temperature. Further discussion about this anomaly will be given in the Section 4.5.2.

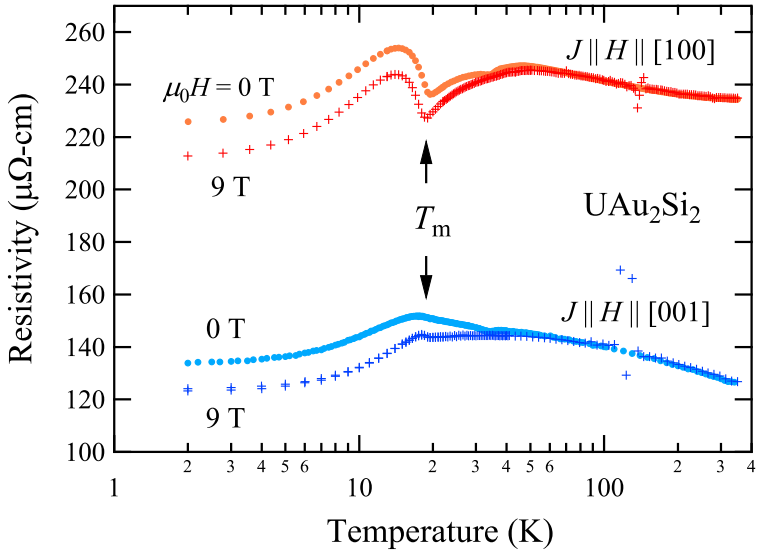

FIGURE 4.3: Temperature dependence of the electrical resistivity of UAu_2Si_2 for electric currents along [100] and [001]. The magnetic field of 9 T was applied along each current direction, namely, the geometry of longitudinal magnetoresistance.

At T_m, the resistivity shows an upturn in both directions of the current. (The upturn in the current along [001] is very subtle, but it does exist.) It means opening of a gap on the Fermi surface due to the phase transition. This kind of anomaly in electrical resistivity suggestive of the reduction of the carrier number is also observed in other uranium 1-2-2 compounds, such as URu_2Si_2, UCo_2Si_2 and UNi_2Ge_2. The temperature dependence of the resistivity below T_m cannot be fitted by a function which contains a term of $\exp(-\Delta/T)$ assuming an opening of a gap of Δ on the Fermi surface, which has given fairly good agreements with the data for URu_2Si_2 and UNi_2Ge_2. Instead, the data on UAu_2Si_2 shows the T^2 dependence below 7 K as shown in Fig. 4.4, which is expected in a Fermi liquid state. We estimated the coefficients A of the T^2 term obtained strongly enhanced values: $A \sim 0.24\ \mu\Omega\mathrm{cmK}^{-2}$ for $J \parallel [100]$ and $A \sim 0.12$

$\mu\Omega\mathrm{cm}K^{-2}$ for $J \parallel$ [001] in zero field. These values yield the Kadowaki-Woods ratio A/γ^2 of $\sim 1.1 \times 10^{-5}$ $\mu\Omega\mathrm{cm(molK/mJ)}^2$ and $\sim 0.5 \times 10^{-5}$ $\mu\Omega\mathrm{cm(molK/mJ)}^2$ for $J \parallel$ [100] and $J \parallel$ [001], respectively, which roughly follow the Kadowaki-Woods relation of typical heavy fermion compounds; $A/\gamma^2 = 1.0 \times 10^{-5}$ $\mu\Omega\mathrm{cm(molK/mJ)}^2$ [89].

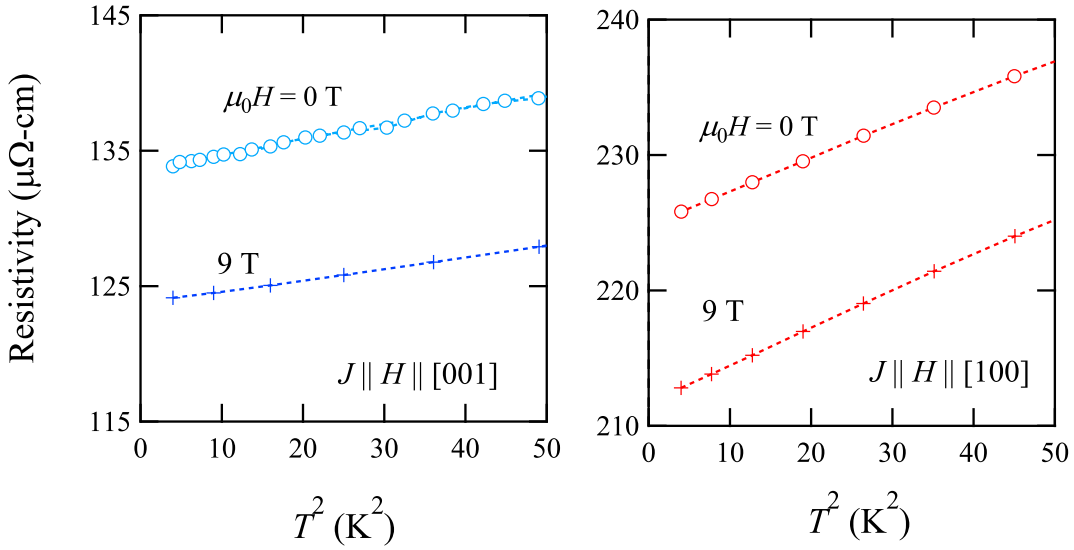

FIGURE 4.4: ρ vs. T^2 plot below ~7 K in current directions of [001] (left) and [100] (right).

4.4.3 Magnetization

The magnetization of UAu_2Si_2 was revealed to have a large anisotropy as presented in Fig. 4.5. The easy axis is the c-axis like most of the other uranium 1-2-2 systems. As we can see in Fig. 4.6, in a higher temperature region above $\sim$ 60 K the magnetization of the both axes follow the modified Curie-Weiss's law, of which expression is

$$\chi(T) = \frac{C}{T - \Theta_W} + \chi_0, \tag{4.1}$$

where χ_0 is a temperature independent term which is considered to include the contributions of Pauli paramagnetism of conduction electrons, diamagnetism of core electrons Van-Vleck term of 5f-electrons, and the background contribution which is considered to come from the GE varnish used to fix the sample. For both the axes, the fitting analyses give small values of χ_0 in an order of 10^{-4} emu/mol. The background is not negligible in the present condition since the sample mass is only 2.8 mg. The effective magnetic moment and the Weiss temperature are estimated as $\mu_{\mathrm{eff}} \sim 3.05(10)$ μ_B/U and $\Theta_W \sim -52 \pm 10$ K for $H \parallel$ [100], and $\mu_{\mathrm{eff}} \sim 2.96(10)$ μ_B/U and $\Theta_W \sim -3 \pm 10$ K for $H \parallel$ [001].

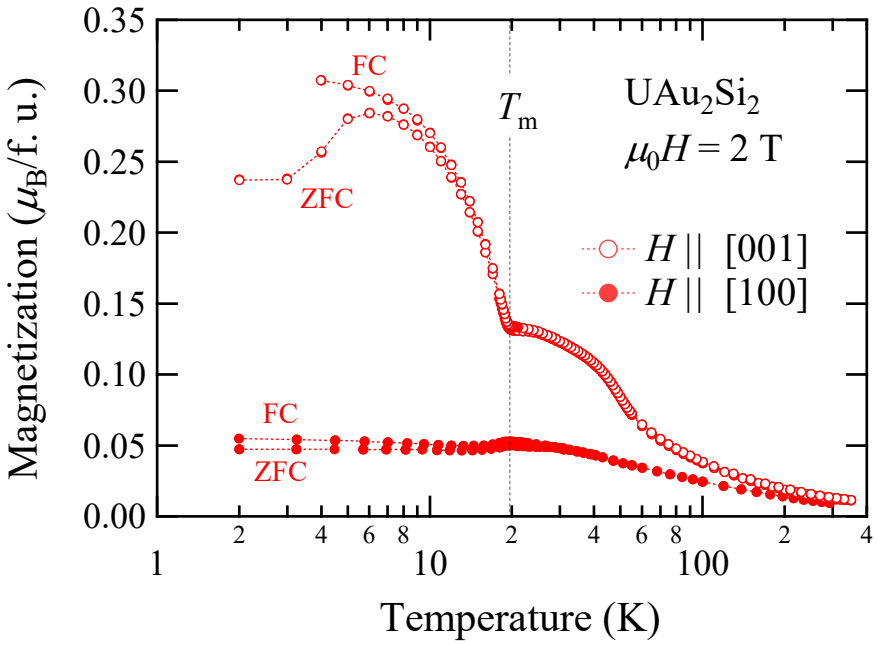

FIGURE 4.5: Temperature dependence of the magnetization of UAu_2Si_2 measured in magnetic field of 2 T. The inset shows the magnetization along [100] in an enlarged scale.

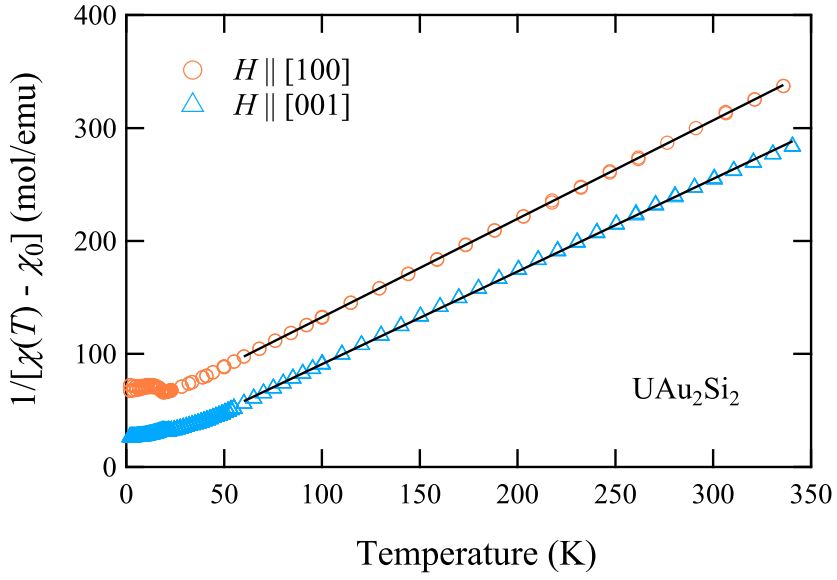

FIGURE 4.6: Temperature dependence of the inverse susceptibility from which the constant contribution is subtracted by using the formula described in the text.

Below T_m, the magnetization shows rather anisotropic behaviors, not only magnitude but also its temperature dependence. It has a large FM upturn only along the [001] axis, which is absent along the [100] axis. The deviation between the FC and ZFC curves becomes more pronounced in both the directions. Similar magnetic irreversibility below the magnetic transition temperature has been reported in some uranium 1-2-2 compounds where the crystal disorder is considered to play an important role. The ZFC curve along the [001] direction shows a complex behavior, which may has some relation to the FM component associated with the phase transition.

The FM-like behavior only along the [001] axis is also shown in the field dependences of the magnetization measured at temperatures lower than T_m displayed in Fig. 4.7. A distinct hysteresis loop is observed in the *M*-*H* curve along the [001] axis, meaning an existence of spontaneous magnetization along this direction, whereas a linear behavior with no hysteresis is observed along the [100] direction. The *M*-*H* curves along the [001] axis measured at temperatures below T_m have step-like anomalies, only when the field increases. Here we define H^* as the field where the step-like anomaly appears. H^* decreases with increasing temperature, and then disappears above T_m. This H^* anomaly suggests a change in the magnetic domain structure of the FM component or a microscopic change in the magnetic structure induced by applying field. It should be confirmed by other experiments including those with microscopic techniques. There is a still a small square-shaped hysteresis even above T_m, 24 K, which is probably related to the FM component as described next.

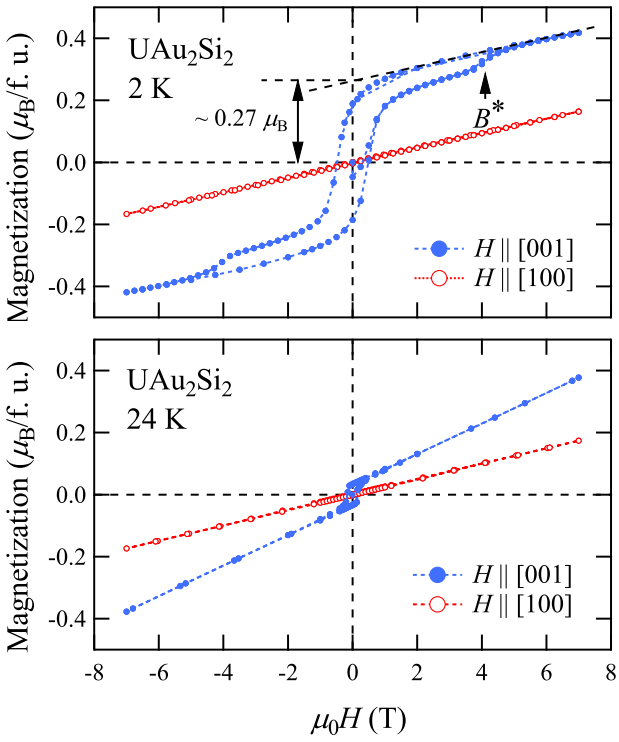

FIGURE 4.7: The magnetization processes in single-crystalline UAu_2Si_2 at 2 K and 24 K.

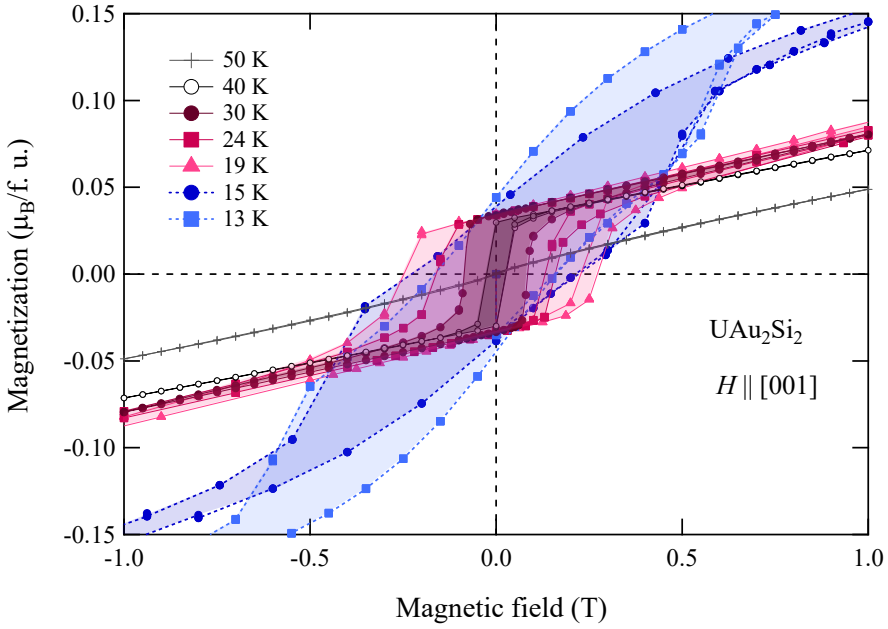

FIGURE 4.8: The hysteresis loops in the magnetization processes in single-crystalline UAu_2Si_2 at several temperature points from 13 K to 50 K.

Around 50 K, an upturn was observed along the both crystallographic axes in the *M-T* curves. The magnitude of the upturn is very small and anisotropic; it is around $0.05\mu_B$ per uranium ion along the [001] and it is less than 0.01 μ_B along the [001]. As shown in the Fig. 4.8, the magnetization curves also show hysteresis loops that indicate spontaneous magnetization arise below ∼50 K. This FM component seems to cause the complex behavior of the ZFC curve in the temperature dependence, of which the field-cooled (FC) curve and zero-field cooled (ZFC) curve deviate from each other below ∼50 K. The possible origin of this FM component will be discussed in the Section 4.5.2.

Figure 4.9 shows temperature dependences of the magnetization measured in higher magnetic fields. The magnetization along the [100] direction simply increases by applying field. On the other hand, the magnetization along the [001] direction shows a cusp anomaly at T_m in magnetic fields above 5 T. The FM like upturn is gradually suppressed by increasing the field above 2 T, resulting in disappearing (or just becoming invisible) above 7 T and simultaneously the cusp anomaly is dramatically enhanced. These anomalous behaviors strongly suggest that the ordered state of UAu_2Si_2 below T_m is not simply FM but including an antiferromagnetic (AFM) component in its ordering structure.

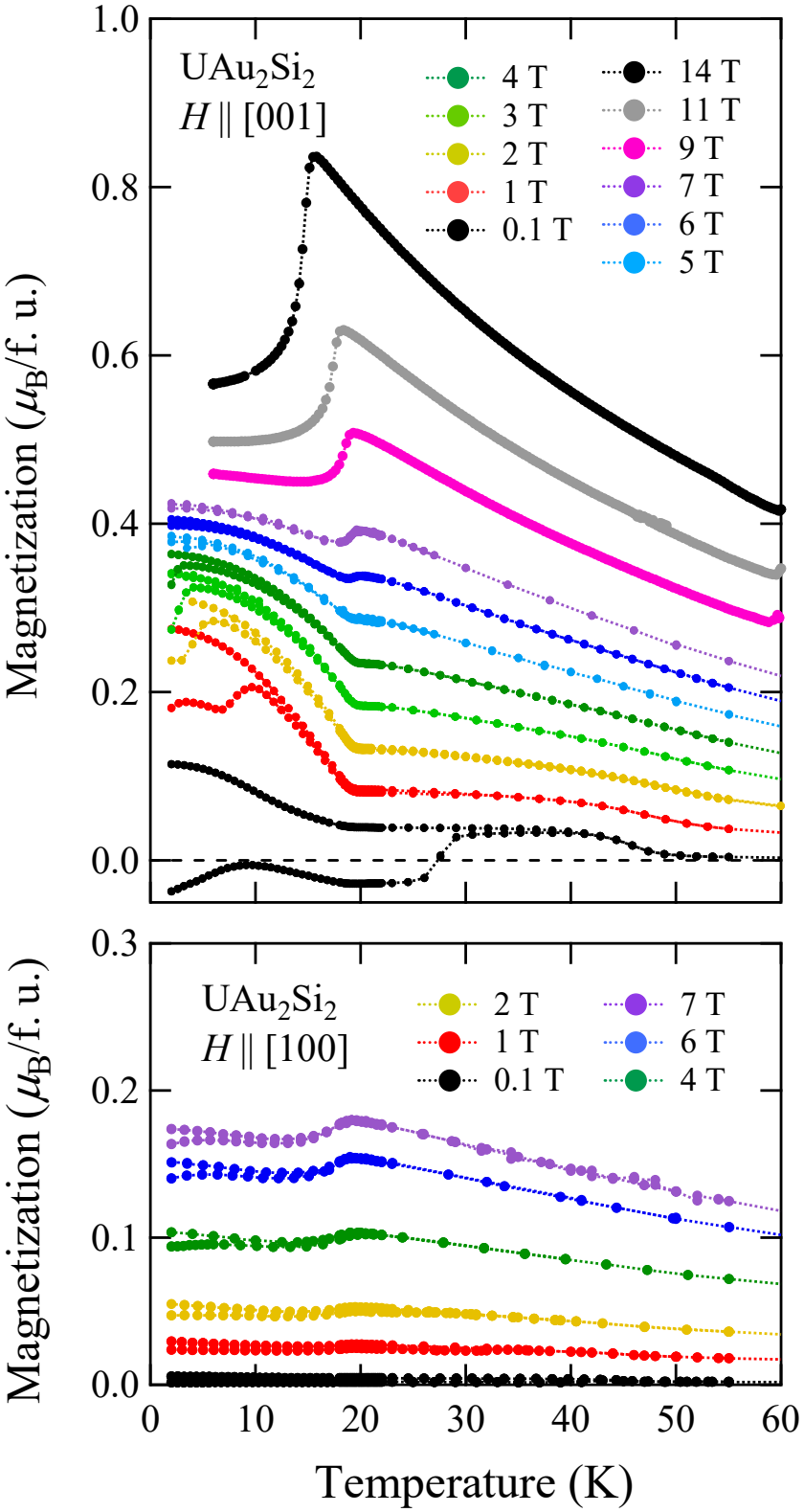

FIGURE 4.9: The temperature dependence of magnetization in UAu_2Si_2 in magnetic fields up to 14 T.

4.4.4 Magnetic field-Temperature phase diagram

We further investigated the magnetization process by extending the measured field range up to 14 T in the [001] direction. The results are shown in Fig. 4.10. We found that below T_m the magnetization curve bends upward in a high-field region. We define H_m as the inflection point of the magnetization curve, which is roughly corespondent to the field where magnetization starts to deviate from a line field dependence as shown in Fig. 4.10. We suggest that the origin of the H_m anomaly is intrinsically different from that of the H^*, because no hysteresis have been observed around H_m unlike around H^*. H_m increases by decreasing temperature down to 4 K, at which H_m reaches $\sim$ 10 T. This anomalous behavior has not been observed at 24 K of above T_m.

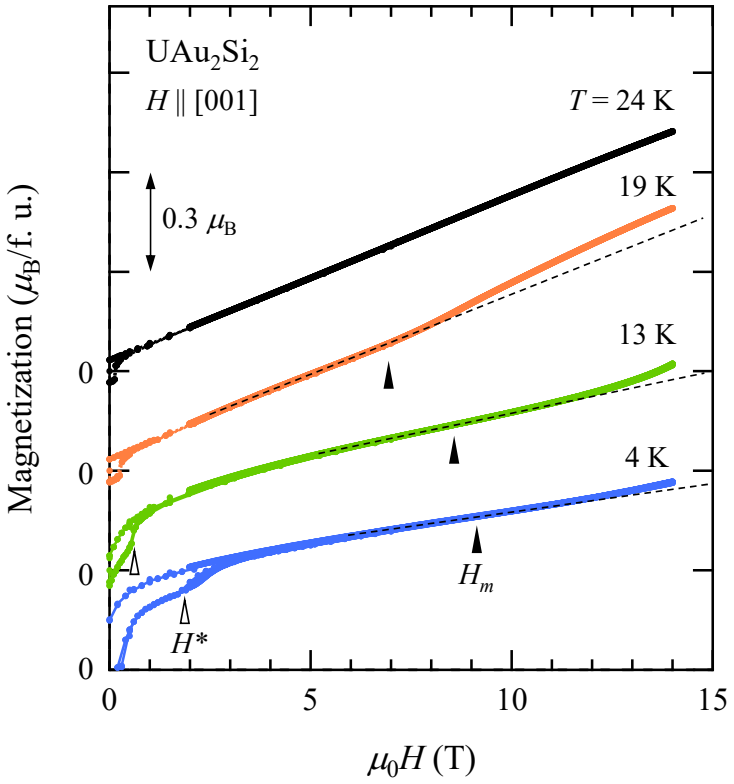

FIGURE 4.10: The magnetization processes in UAu_2Si_2 up to 14 T along the [001] direction. The broken line is a guide to the eye.

We have constructed in Fig. 4.11 a magnetic field-temperature $H-T$ phase diagram of UAu_2Si_2 for the applied field along [001] direction. T_m was determined from the temperature dependences of specific heat and magnetization in a magnetic-field range from 0 to 9 T and 9 to 14 T, respectively. It is found that T_m goes up as the magnetic field increases in a low field range below $\sim$ 5 T. This provides a remarkable contrast to the behavior of usual AFM compounds, where Néel temperature decreases when applied magnetic field is increased. It is probably related with the uncompensated spin components. In the higher magnetic field above 5 T, T_m decreases as the field is increased. In order to see where the phase-boundary line towards, the experiments in higher magnetic fields is necessary.

Since we do not know whether the H_m corresponds to a phase boundary or not at the present stage, we would like to refer to the two areas in the phase diagram divided by H_m as Area I and Area II, respectively. Combined with the results of magnetization measurements shown in Fig. 4.10, it is found that the FM component appears only in the Area I. Furthermore, H_m seems to appear just from the maximum of T_m; some sort of properties of the ordered state might be changed in the Area II above this maximum point. These facts suggest that the nature of the magnetically ordered state may differ between the Areas I and II.

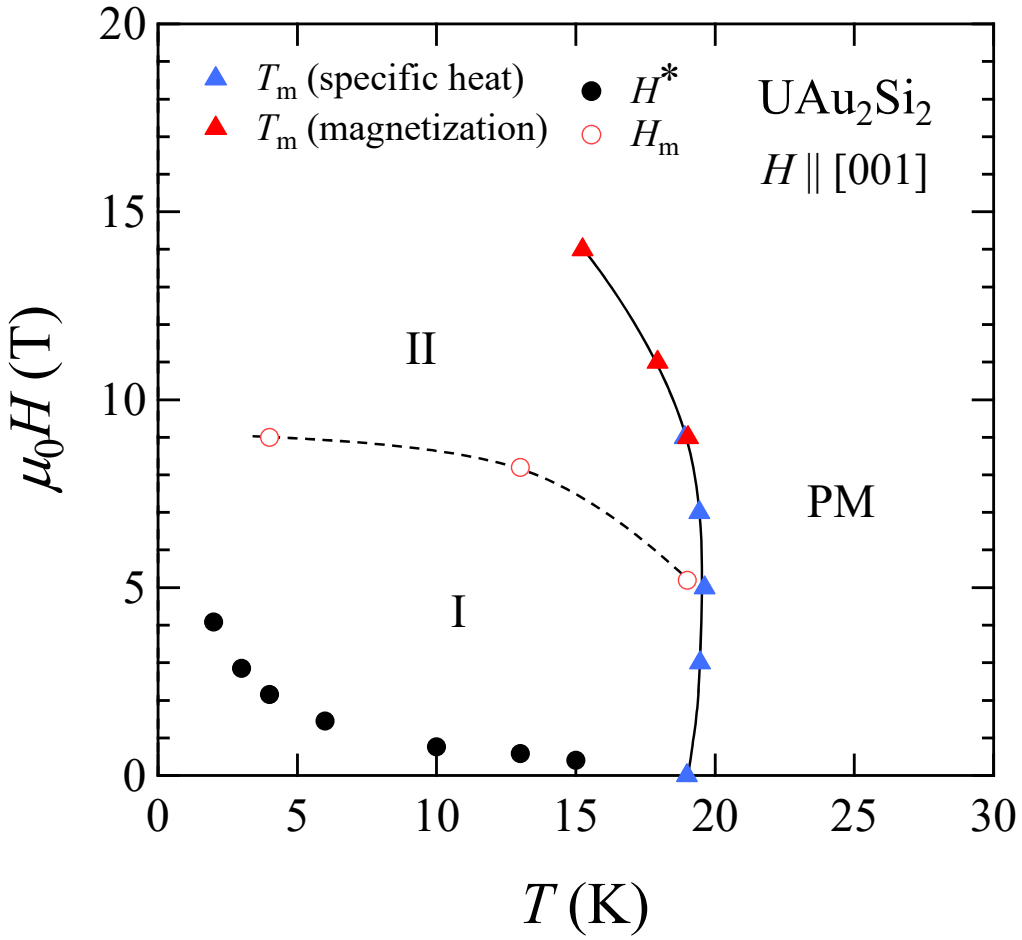

FIGURE 4.11: The $H - T$ phase diagram of UAu_2Si_2. The magnetic field is along the tetragonal [001] direction. The broken line is a guide to the eye.

4.4.5 Magnetic-entropy analysis

For investigation of the magnetic entropy of 5f electrons in UAu_2Si_2, we measured specific heat of polycrystalline samples of $ThAu_2Si_2$ and UAu_2Si_2. Figure 4.12 shows the temperature dependence of 5f-electronic contribution of the specific heat and magnetic entropy of UAu_2Si_2, obtained by subtracting the specific heat of $ThAu_2Si_2$ from that of UAu_2Si_2. The magnetic entropy reaches $\sim R\ln 2$ just above T_m, and reaches $\sim R\ln 6$ at room temperature. A distinct peak anomaly in the specific heat associated with the phase transition can be seen at T_m, giving the evidence that the phase transition is caused by 5f electrons of uranium ions. The released entropy at the transition is estimated to be only $\sim 0.2R\ln 2$, if one assumes entropy balance based on the itinerant picture. The rest of the magnetic entropy results in the large electronic specific heat coefficient of $\gamma \sim 180$ mJ/K^{2}mol.

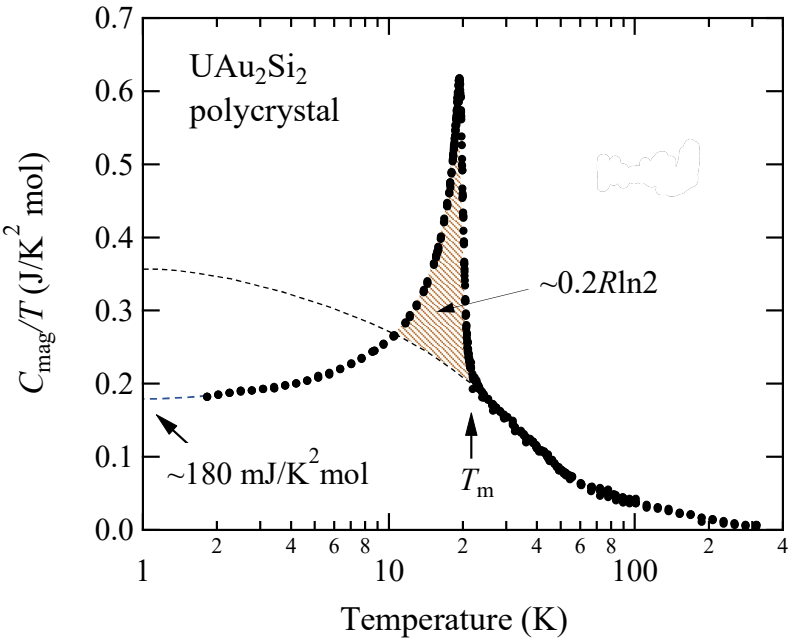

FIGURE 4.12: The 5f electronic contribution to the specific heat of UAu_2Si_2 derived by subtracting the $ThAu_2Si_2$ data.

4.4.6 ^{29}Si-NMR

Figure 4.13 exhibits ^{29}Si-NMR spectra at the fixed frequency of 38.5 MHz obtained by sweeping the magnetic field parallel($H_{\parallel}$) and perpendicular($H_{\perp}$) to the magnetically-easy axis, namely, the c-axis. Since ^{29}Si nuclei have spin 1/2, the NMR spectra has a single peak in a paramagnetic state. In this condition, the resonance field of the naked Si nucleus spin is calculated as $H_0 = 38.5/\gamma \sim 4.55$ T. As shown in Fig. 4.14, the observed peaks of NMR spectra in the fields of $H_{\perp}$ and $H_{\parallel}$ show a good separation from each other. This means that the present powdered sample is successfully oriented.

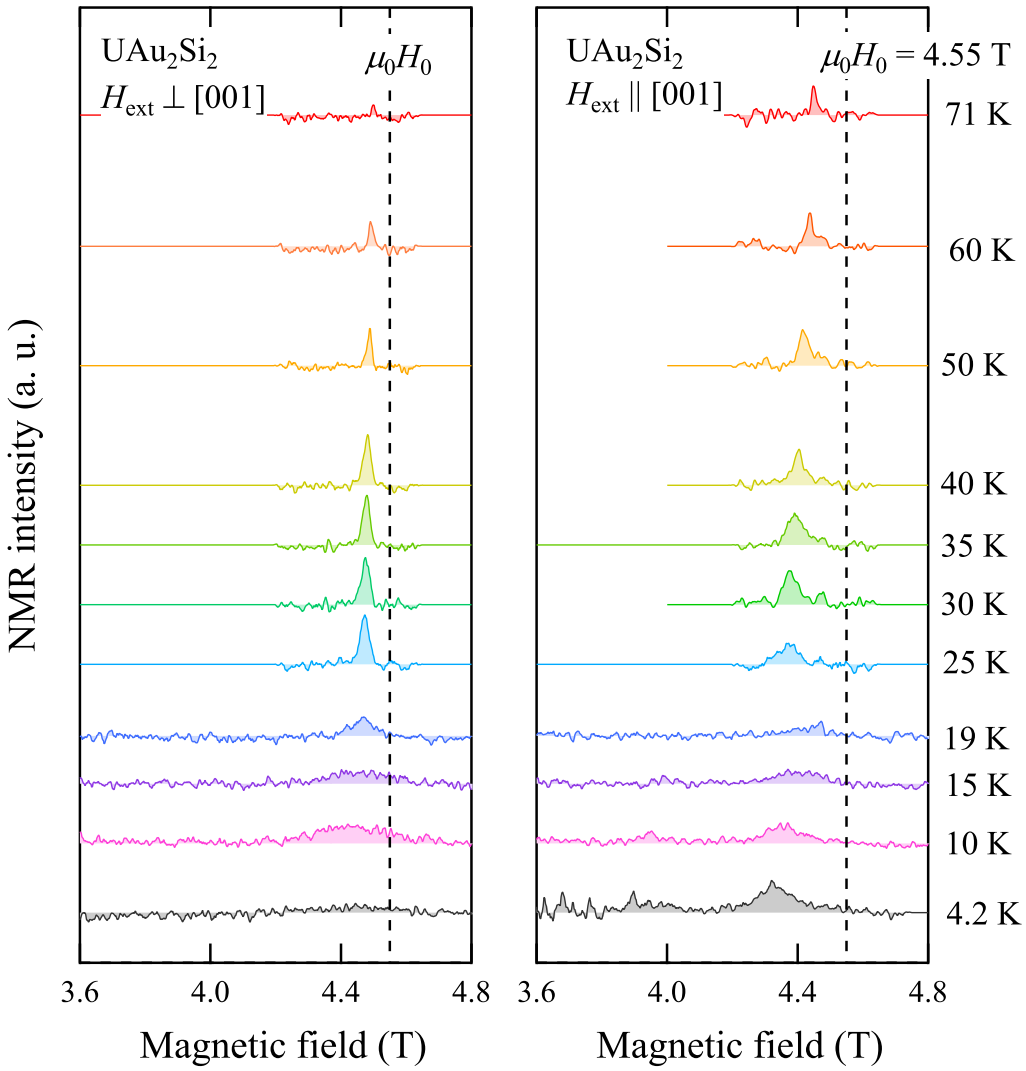

FIGURE 4.13: ^{29}Si-NMR spectra of the UAu_2Si_2 powdered polycrystalline sample. The broken line denotes the resonance field expected for a free Si atom; $\mu_0 H_0 = 4.55$ T.

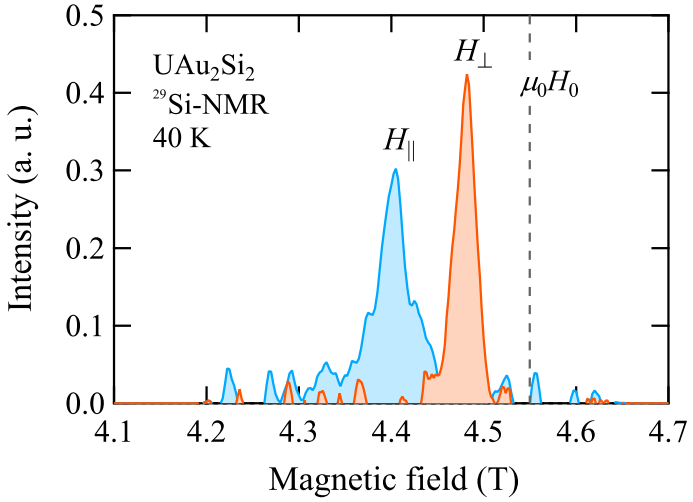

FIGURE 4.14: Typical spectra of ^{29}Si-NMR of the magnetically oriented powdered sample of UAu_2Si_2 measured at 40 K in the magnetic fields parallel and perpendicular to the c-axis.

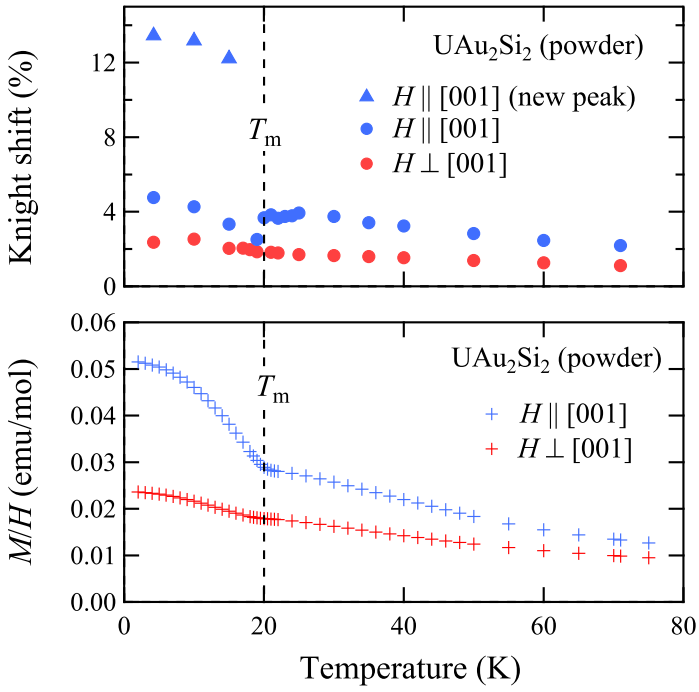

FIGURE 4.15: Temperature dependences of the Knight shift (top) and magnetic susceptibility (bottom) of the oriented powdered sample.

The transverse and longitudinal components of Knight shift, $K_\perp$ and $K_\parallel$, were evaluated at the center of resonance peaks determined by peak fittings using the Gaussian function. Plotted in Fig. 4.15 are temperature dependence of $K_\perp$ and $K_\parallel$, which are similar to the behavior of the magnetization. Above T_m, we observed linear relations between the Knight shifts and the magnetic susceptibility as shown in Fig.4.16. From the slope of these $K - \chi$ plots, the spin hyperfine coupling constants are estimated as $A_\parallel \sim 6.9$ kOe/μ_B and $A_\perp \sim 4.8$ kOe/μ_B. They are of the same order of magnitude as those of some isostructural relatives: $A_\mathrm{isotropic} \sim 3.6$ kOe/μ_B of URu_2Si_2 [90], $A_\mathrm{ab} \sim 2.84$ kOe/μ_B of $CePd_2Si_2$ [91].

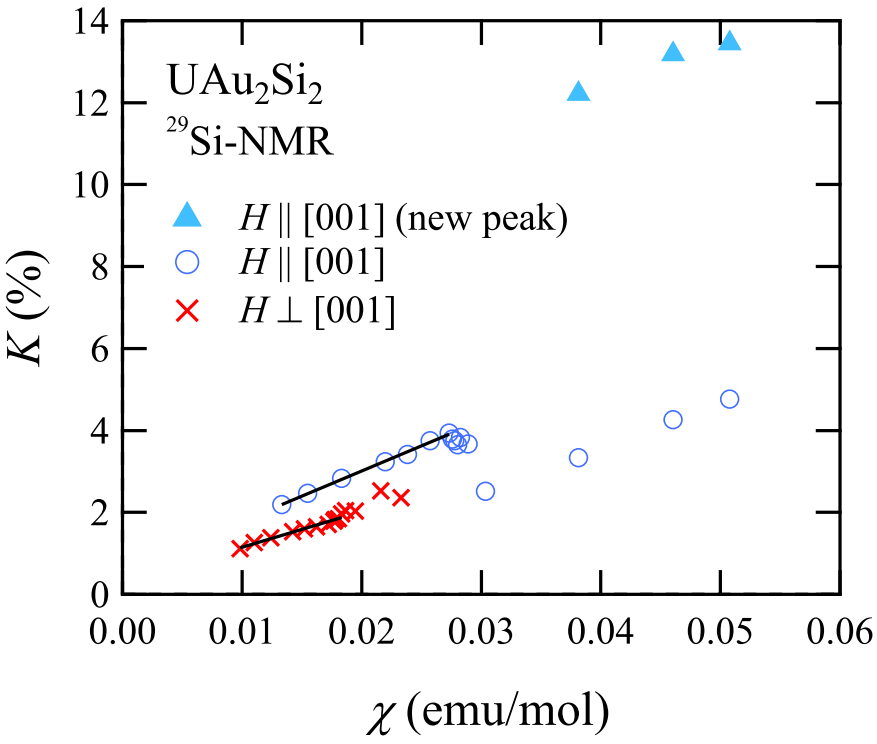

FIGURE 4.16: Knight shift vs. magnetic susceptibility of the oriented powdered sample. The solid line is the least-square fit within the paramagnetic state.

Upon cooling, the observed peaks become broader just above T_m, indicating the development of short-range order of the magnetic transition. Below T_m, we observed a distinct difference between spectra measured in the two directions of magnetic fields; in $H_{\parallel}$ a small new peak appears in the lower fields, while in $H_{\perp}$ the resonance peak just becomes broader (see Fig. 4.17). This is a direct evidence of an occurrence of an AFM order with at least two sublattices, and is consistent with the results of magnetization measurements described above. The profile measured at 4.2 K in $H_{\parallel}$ was analyzed by using the lorentzian fitting to obtain the intensities of each peak as shown in Fig. 4.18. This analysis gives the intensity ratio of $I_{\mathrm{small}} : I_{\mathrm{large}} \sim 1 : 2$, where I_{small} and I_{large} are intensities of the smaller peak at ~ 3.9 T and the larger one at ~ 4.3 T, respectively. The parameters obtained by the fitting are listed in Table 4.2. The intensity ratio of 1 : 2 means that there are two kinds of Si sites with non-equivalent component of internal fields projected on the c-axis in the ordered state, and this strongly suggests an AFM order occurring with an ordering period as long as three times of a period of the crystal lattice.

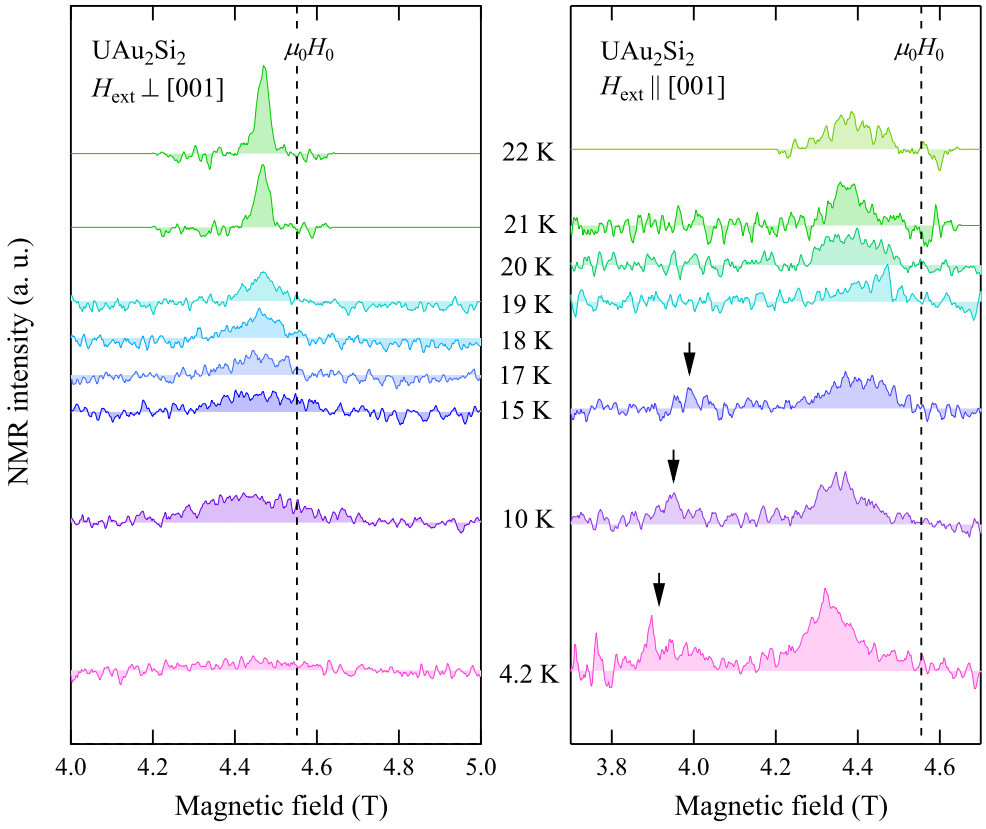

FIGURE 4.17: Enlarged view of the ^{29}Si-NMR spectra of the UAu_2Si_2 powdered sample in the low temperature region below 22 K.

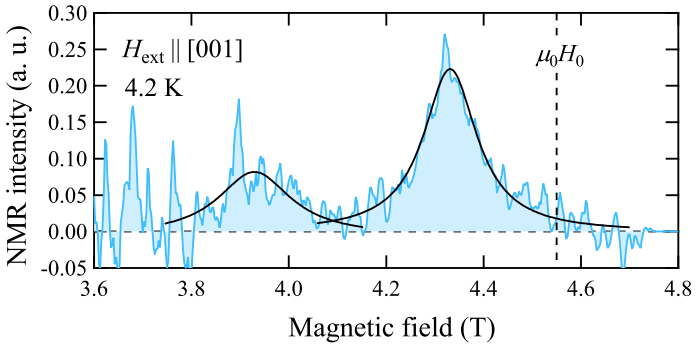

FIGURE 4.18: ^{29}Si-NMR spectra of the UAu_2Si_2 powdered sample measured at 4.2 K for fields parallel to the c-axis. Solid curves indicate the best fits of the data using the Lorentzian function with parameters summarized in Table 4.2.

TABLE 4.2: Magnetic field of peak center, $H_{\rm reso}$, the mean value of internal fields, $\Delta H (\equiv H_0 - H_{\rm reso})$, the full width at half maximum (FWHM), the signal intensity, $I_{\rm reso}$, obtained by the fitting analysis of the ^{29}Si-NMR spectra taken at 4.2 K.

peak notation	$H_{\rm reso}(T)$	ΔH (T)	FWHM (T)	$I_{\rm reso}$ (a. u.)
small peak	3.94	0.62	0.18	0.016
large peak	4.33	0.22	0.13	0.030

The large broadening of spectra in $H_\perp$ below $T_{\rm m}$ also indicates that there are finite internal fields in the basal plane generated by a magnetic phase transition. One might think that the broad shape of the spectra for $H_\perp$ below $T_{\rm m}$ is due to the distribution of misorientation of the powdered crystals. However, the observed peak broadening cannot be explained only by the effects of misorientation, because the mixing of the c-component of the internal field can not give any intensities in the higher fields range above H_0, contrary to the present observation.

4.5 Discussion

4.5.1 Consideration of possible magnetic structure

Now let us consider what kind of the magnetic order in UAu_2Si_2 on the basis of the results of NMR measurements. The main results are summarized as follows: (i) In the ordered state, there are two kinds of Si magnetic sites at which the c-component of the internal fields is non-equivalent. (ii) The ratio of the site number is about 1 : 2. (iii) The component of the internal fields in the c-plane also has a non-zero value. Here we employed the symmetry analysis of the hyperfine field for several AF spin structures, and finally deduced that the most possible structure to explain the observed NMR spectra is the uncompensated AFM with $\boldsymbol{q} = (2/3, 0, 0)$ and magnetic moments pointing along the c-axis. The details of this analysis are presented in Appendix A.1. We have

assumed that effective internal fields at the Si sites are the sum of the transferred hyperfine fields from five U neighbor ions, the temperature-independent hyperfine fields from Pauli paramagnetic and Van-Vleck contributions, and the dipolar fields. The diamagnetic component is neglected. Assuming also the localized 5f moments, we have estimated the magnitude of the ordered moment $m_{\rm ord} \sim 1.4\ \mu_{\rm B}$.

In spite of the simplicity of the analysis, the deduced magnetic spin structure with $\boldsymbol{q} = (2/3, 0, 0)$ is roughly consistent with the results of the magnetization measurements on the single crystal presented above. It can be considered that the magnetization curve along the [001] axis at 2 K is composed of the FM saturation component of $m_{\rm s} \sim 0.27\mu_{\rm B}$/U and a linear component which is proportional to magnetic field as shown in Fig.4.7. If the above spin structure is realized, the net component of the spontaneous magnetization per U atom should be one-third of the magnitude of the ordered moment. The ordered moment can thus be estimated from the magnetization measurements as $3m_{\rm s} \sim 0.81\ \mu_{\rm B}$/U, which is of the same order as $m_{\rm ord}$ deduced from the NMR results. The difference between two estimates can be attributed mainly to our simple assumptions in the analyses for the NMR spectra, such as the limited number of considered neighbors, site-independent magnitude of the local moments in the finite field, neglects of the effects of diamagnetic fields and misorientation, and so on. NMR and neutron-scattering measurements on a single-crystalline sample will also be desired to proceed further with the discussion.

It is interesting to note that the same magnetic structure is realized in the so-called phase II of URu_2Si_2, which appears when a high magnetic field of $\sim$ 35 T is applied to the c direction of the system [92]. Because the phase II is neighboring to the HO phase of URu_2Si_2, it may provide useful information about the HO to study in detail the AFM phase in UAu_2Si_2. In particular, it will be interesting to examine what type of interactions provokes the system to order in this structure, which breaks 4-fold symmetry in the c-plane. No other system in the UT_2Si_2 family does not break the in-plane symmetry in zero magnetic field, showing strong FM coupling in the basal plane. Of course, since the present NMR measurements were performed in the magnetic field of $\sim$ 4.5 T, we cannot be sure precisely about the magnetic structure at zero field. As mentioned before, the H^* anomaly in the magnetization of the single-crystalline sample might suggest a change of the magnetic structure induced by magnetic field. Neutron diffraction experiments in zero field will be one of the primary future work also in this respect.

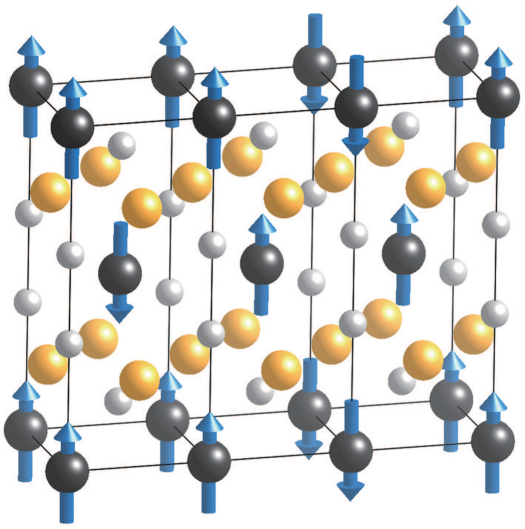

FIGURE 4.19: Magnetic structure speculated from the ^{29}Si-NMR experiments. The propagation vector $\boldsymbol{q}$ is (2/3, 0, 0), and the magnetic moments is pointing along the *c*-axis.

Here we have discussed the simplest case of the magnetic structure of UAu_2Si_2, with each well-localized magnetic moment pointing to the *c*-axis. Even though this hypothesis gives fairly good semi-quantitative descriptions to understand the present results of the NMR experiments and the magnetization measurements, of course we still cannot rule out the possibility that the moments are tilted from the *c*-axis. Particularly, the present NMR experiments were performed on the powdered sample, providing only a few, limited pieces of information about the way in which the basal plane components of magnetic moments are arranged. The tilted ordered moments can be expected from the almost isotropic effective moments deduced from the susceptibility measurements. On the condition that a canted AFM order, such as a helical magnetic order, occurs in this compound, applying magnetic field parallel to the *c*-axis is expected to make the angle between magnetic moments and the *c*-axis smaller. It may account for the augmentation of the entropy released at T_{m} by applying magnetic field only along the *c*-axis.

4.5.2 FM component above T_{m}

Here we discuss whether the FM component at around 50 K is an intrinsic sign of change in the magnetic ordered state of UAu_2Si_2 itself. The simplest explanation of its origin is that this weak FM component is extrinsic, possibly due to FM impurities or a second phase with different chemical component from UAu_2Si_2, because no anomaly was observed around 50 K in the specific heat. In addition, the magnitude of the FM

components shows a large sample dependence when compared with the previous reports. The extrinsic FM components have been observed in other uranium 1-2-2 systems such as URu_2Si_2 and UNi_2Ge_2, whose magnetization shows FM anomalies just below their bulk phase transitions with a large anisotropy, without any anomalies in other bulk properties [93, 94]. Such the parasitic FM components might be one of the common characteristics of uranium 1-2-2 systems, and possibly that of UAu_2Si_2 may also be one of them.

However, the *M-H* curves show a puzzling behavior as shown in Fig. 4.8. Below 50 K, a square-shaped hysteresis loop appears and gets wider by decreasing temperature down to $T_{\rm m}$ = 19 K, and suddenly changes its shape dramatically below $T_{\rm m}$. It is striking that the square hysteresis due to the FM contribution above T_m appears to vanish below $T_{\rm m}$, highlighted by the fact shown in Fig. 4.8 that the width of hysteresis, corresponding to the coercive force, is smaller in the ordered state, at 15 K, than just below $T_{\rm m}$, 19 K. If it has its origin in the extrinsic FM impurities, the hysteresis should survive, independently of the ordered state of UAu_2Si_2. This experimental fact may suggest that some sort of weak magnetic order intrinsically occurs in UAu_2Si_2 at around 50 K. Then it is considered that only a tiny fraction of the degrees of freedom which magnetic moments of U ions have orders at $\sim$ 50 K, and the phase transition at T_m is caused by the rest of them. For instance, one of the possible scenarios is that, a canted ferromagnetism whose spontaneous magnetization is along to the [001] direction, occurs at around 50 K, leaving the basal-plane components of the magnetic moments paramagnetic. Perhaps the dip-like anomaly in the resistivity at 34 K has some connection with this FM component. In fact, the ZFC curve of magnetization in the weak field of 0.1 T shows an steep reversal of its sign at around 30 K (Fig. 4.9), indicating FM-domain flipping, which may affect the resistivity.

The 50 K anomaly was reported by three previous studies made by Rebelsky *et al.*[26], Torikachvili *et al.*[86], and Lin *et al.*[20], all of which were made on annealed polycrystalline samples. Rebelsky *et al.*, who performed powder neutron diffraction and magnetization measurements, reported that intensity of the neutron diffraction at several Bragg spots suddenly change at around 50 K but no superlattice reflection was found. They also observed the FM-like anomaly in the magnetization. The saturation magnetization estimated from the magnitude of the upturn in the *M-T* curve is $\sim$ 0.01 $\mu_{\rm B}$ per uranium ion in field of 1000 Oe. This value has the same order of that of the present sample, $\sim$ 0.05 $\mu_{\rm B}$ per uranium ion, although we cannot simply compare them because one is a polycrystalline sample and the other is a single-crystalline sample. Lin *et al.* also observed an upturn behavior at $\sim$ 50 K in the magnetization measurements, without any anomalies around this temperature in the specific heat and electrical resistivity. The saturation magnetization is estimated to be $\sim$ 0.001 $\mu_{\rm B}$ per uranium ion in field of 20 Oe, which is quite small. The difference of those values between reports by Rebelsky and Lin might come from sample dependence and difference between the measuremental conditions. Torikachvili *et al.* performed the ac susceptibility measurements, where a sharp peak was observed at 44.3 K. The peak is immediately suppressed by applying magnetic field of 2.1 kOe, and the authors concluded that this suggests an existence of weak ferromagnetism. On the other hand, they did not find any anomalous behavior at this temperature in the electrical resistivity measurements. In order to clarify the origin of these anomalies, further investigation of sample dependence and measurements of other physical properties, particularly by means of microscopic techniques such as neutron diffraction, are necessary.

4.5.3 5f-electronic properties

Here, we discuss the 5f electronic properties in UAu_2Si_2. We observed the almost isotropic effective magnetic moments and the magnetic entropy that reaches $\sim R\ln 6$ at room temperature. These experimental facts suggest that the smaller crystalline-electric-field (CEF) energy scale than the other uranium 1-2-2 compounds. The magnetically isotropic feature provides remarkable contrast with the fact that not a few UT_2Si_2 compounds exhibit strong uniaxial magnetic anisotropy. URu_2Si_2, UPd_2Si_2, and UCr_2Si_2 are such the typical examples, in which the [001] axis is the easy axis, and the a-axis magnetic susceptibility shows very weak temperature variations [4, 10, 95]. Correspondingly, the magnetic entropy at room temperature is relatively large, when compared with, *e.g.* $\sim R\ln 3$-$\sim R\ln 4$ of the Ising system URu_2Si_2.

We now consider two main influential factors in the CEF effects in the UT_2Si_2 system. In general, the CEF effects are effectively composed of the static electric field generated by surrounding ions, which is usually treated by a point-charge model, and the hybridization effects between the f-electrons and the non-f ligands. One important factor which directly governs the static electric field is the distance between f-ions and the non-f ligands, which can be tuned by the lattice parameters, the a and c parameters in the case of the tetragonal structure. It also affects the hybridization; the smaller distance makes the hybridization stronger. Another factor is the number of d-electrons of the transition-metal ions. Some previous reports suggested that the increase of the d-band filling weaken the d-f hybridization, because the energy of d-band is considered to be pulled down away from the Fermi level by increasing the filling, resulting in the less overlap of the d and f bands [96, 97]. Since UAu_2Si_2 has the largest lattice parameter of $a \sim 10.3$ Å and the largest d-band filling in the 5d systems of UT_2Si_2, the smaller CEF effect can be expected. This speculation is consistent with the present results just mentioned above. Note that UCu_2Si_2, which is under the similar condition to UAu_2Si_2 in the 3d systems, also has almost isotropic effective moments and large magnetic entropy at room temperature of $\sim R\ln 9$ [8].

A local character of the 5f electrons can be seen in the magnetic susceptibility, which follows the Curie-Weiss law at high temperature above ∼60 K. Moreover, the resistivity shows the -ln$T$ behavior from room temperature down to ∼ 60 K. If this is due to the Kondo effect, this also means existence of local magnetic moments. On the other hand, at lower temperature the 5f electrons behave like itinerant electrons, as seen in the large γ and A values, with which we can put UAu_2Si_2 on the Kadowaki-Woods plot for the typical heavy fermion compounds, $A/\gamma^2 = 1 \times 10^{-5}\mu\Omega\mathrm{cm(Kmol/mJ)}^2$. Although these values should be interpreted carefully, because they are deduced from the data below the transition temperature, these experimental facts strongly suggest that the low-temperature state of this compound is described by the Fermi-liquid theory with heavy 5f itinerant electrons.

4.5.4 Instability of crystal structure

In the last part, we refer to the crystallographic disorder. For some related compounds, a crystallographic disorder has been discussed. For instance, it has been reported that in URh_2Ge_2 its magnetic ground state can be tuned between the spin glass order in an as-cast sample and a long range magnetic order in an annealed sample, by removing a crystallographic disorder with annealing [98, 99]. The disorder is established by the

random mixing of the Rh and Ge atoms over their available lattice sites. A similar mixing disorder is also considered to take place also in UIr_2Si_2, which orders antiferromagnetically below 6 K [17]. In this compound it is pointed out that about 6 percent of all the Ir sites are substituted. The disorder contributes to large residual resistivity of ~ 90 $\mu\Omega$cm. For UPt_2Si_2, another type of disorder has been indicated, which results from a static and random displacements of the Pt and Si atoms within the tetragonal ab-plane [19]. As their common characteristics, they exhibit very large values of the residual resistivity, possibly reflecting existence of the non-negligible disorder. There are also other various related systems of UT_2X_2 (T = Co, Ni, Rh, Pd, X = Si, Ge) which have very large residual resistivity [15, 94, 100, 101]. The unusually large residual resistivity of UAu_2Si_2 observed in the present study might be attributed to a similar disorder.

It has been pointed out that the UT_2X_2 systems seem to always have a structural instability originated from a competition between crystallization in the $ThCr_2Si_2$ (I4/mmm) and $CaBe_2Ge_2$ (P4/nmm) typed structure [19]. In fact, it has been reported that UCo_2Ge_2 crystallizes in a structure with symmetry lower than I4/mmm and it changes into the $ThCr_2Si_2$ typed one by the annealing [102]. Another example of this kind of the competition can be seen in an isostructural Ce-system $CeIr_2Si_2$, which adopts those two type of structure depending on an annealing procedure [103]. We imagine that UAu_2Si_2 is just on the boundary between these two kind of the structures, which might make it difficult to obtain single-phased samples, resulting in the difficulty of single crystalline growth. Unfortunately, a quantitative discussion of the disorder cannot be made at the present moment because the powder XRD patterns or the oscillation photographs of the single crystal have not achieved the accuracy required for the refinement of the occupancy parameters. The higher resolution of diffraction experiments and better-quality samples are needed for the detailed investigation of the disorder.

It would be also interesting if the large γ-value is realized only in the sample with a larger crystal disorder. The large disorder might prevent the residual degree of freedom of the 5f electrons from ordering even below $T_{\rm m}$, concealing the real nature of the ground state. A crystal with less disorder may give us a chance to see it. Search for more appropriate sample growing condition to improve the sample quality should be one of the most important challenges for the future.

4.6 Conclusions

We have succeeded in single crystal growth of the uranium intermetallic compound UAu_2Si_2 for the first time, and measured the specific heat, electrical resistivity and magnetization. We also performed ^{29}Si-NMR measurements on the polycrystalline sample of this compound for the first time. The results of the NMR experiments strongly suggest that the spin-uncompensated AFM order with q = (2/3, 0, 0) takes place below $T_{\rm m} = 19$ K, not the FM order so far believed as the nature of the order. The magnetization of the single crystal is also consistent with this structure. From the entropy analysis it is considered that the itinerant 5f electrons get involved in the phase transition, while the magnetic ordering structure can be explained semiquantitatively by the simple local spin model. Further analyses of the local spin model with intersite interactions may give a useful information. A crystallographic disorder might play an significant role in its low-temperature physical properties like other related 1-2-2 systems, with competition of two types of different crystal structure. Improvement of the quality of the single-crystalline samples and microscopic experiments to determine the magnetic structure are essential for further research.

Chapter 5

Concluding remarks

In this work, we investigated two kinds of phase transitions whose order parameters were unclear. First, the crystal-structural 4-fold rotational symmetry in the hidden order (HO) of URu_2Si_2 was examined by means of the backscattering X-ray diffraction experiments with the highest resolution ever applied to this compound. In consequence, the following results were obtained:

- The 4-fold rotational symmetry about the tetragonal c-axis remains unbroken in the temperature range from 30 K to 6 K within the experimental accuracy that the orthorhombicity is smaller than $\epsilon = |b' - a'|/(b' + a') < 3 \times 10^{-5}$, even if it exists.
- The present sample of RRR $\sim$ 20 shows a good agreement with the previously reported thermal expansion data, ensuring that the sample certainly goes through the HO phase transition. From this result and consideration of the Grüneisen's relationship, we conclude that the lattice distortion reported in a high-RRR sample is not an intrinsic property of the HO.
- The distribution of the lattice parameter, a, has been observed, for the first time, on this compound. It is indicated that the present sample is composed of several crystal grains with the coherence length of ~ 1 μm and the mean lattice parameters of each grain are in the range $\Delta a/a < 1.2 \times 10^{-4}$.

Secondly, we investigated the low-temperature magnetic properties of UAu_2Si_2, in order to clarify the nature of the magnetic phase transition at 20 K. We succeeded in growing single-crystalline samples of this compound, for the first time. The magnetic, thermal, and transport properties were studied by means of magnetization, specific heat, and electric resistivity, and the ^{29}Si-NMR experiments. The obtained results are summarized as follows:

- The AFM order, with $\boldsymbol{q}$ = (2/3,0,0) and the ordered moment of $\sim$1 μ_B, is possibly realized below 20 K. This is the same magnetic structure as that in the phase II of URu_2Si_2, which appears in a high-field region just after the suppression of the HO by the first meta-magnetic transition.
- The energy scale of the crystalline electric field for this compound is relatively small in the UT_2Si_2 systems; the magnetic entropy reaches $\sim R$ln6 at room temperature and the magnetic susceptibility does not show the Ising anisotropy, like the other 1-2-2 systems yielding the almost isotropic effective moments.
- The large electronic specific-heat coefficient γ and quadratic coefficient of electrical resistivity A were obtained even in the ordered phase. The combination of the γ $\sim$150 mJ/K^{2}mol and the $A \sim 0.24$ $\mu\Omega$cmK^{-2} follow the Kadowaki-Woods relation for typical heavy-fermion compounds.

- The present samples showed an instability of the crystal structure through the crystal growing processes, which might lead to the difficulty in the single-crystalline growth. It may all be the reason for the large residual resistivity.
- The magnetic field-temperature phase diagram was constructed within the field range up to 14 T. It implies the existence of multiple magnetic phases like UPd_2Si_2.

On the basis of the present study together with the previous reports on URu_2Si_2, we propose a possibility of a $\boldsymbol{q} = 0$ first-order phase transition as a candidate for the HO, because no evidence of symmetry breaking by the HO has been detected. It might be also useful to have a closer look at the magnetically ordered phase of UAu_2Si_2 to exploit information leading to solution of the HO mystery. UAu_2Si_2 can be considered to be one of the systems where an order of local magnetic moments and itinerant component behaving like Fermi liquid coexist, which is more distinct than UPd_2Si_2 and UPt_2Si_2. As a future work, we are going to make a phenomenological analysis based on a local-spin model to test whether the phase diagram is reproduced or not.

Appendix A

Analysis of ^{29}Si-NMR Spectra of UAu_2Si_2

A.1 Tensor notation of the hyperfine field

To discuss the spin structure of UAu_2Si_2 below T_m, we first consider symmetry of the hyperfine coupling tensor. The internal field $\boldsymbol{H}_{\rm int}$ that contributes to the NMR of the Si nucleus is considered to be composed of the following three contributions:

$$\boldsymbol{H}_{\rm int} = \boldsymbol{H}_{\rm hf} + \boldsymbol{H}_{\rm dip} + \boldsymbol{H}_{\rm dia}, \tag{A.1}$$

where $\boldsymbol{H}_{\rm hf}$, $\boldsymbol{H}_{\rm dip}$ and $\boldsymbol{H}_{\rm dia}$ are the hyperfine field, the dipolar field produced by the local magnetic moments and the diamagnetic field, respectively. Firstly for the rough estimation, we assume that the long-range dipolar interaction and the diamagnetic field give only small contribution to the internal field, and consider only the short-range transferred and on-site hyperfine interactions between Si nucleus and the ordered moments on the four first-nearest-neighbor and one second-nearest-neighbor U sites. Now we refer to the first-nearest neighbor sites and the second-nearest neighbor site as sites (1) and site (2), respectively as displayed in Fig. A.1.

Then, the internal field can be rewritten as

$$\boldsymbol{H}_{\rm int} = \boldsymbol{H}_{\rm hf} = \sum_{i}^{4} A_i^{(1)} \boldsymbol{m}_i^{(1)} + A^{(2)} \boldsymbol{m}^{(2)}. \tag{A.2}$$

where $A_i^{(1)}$ are the hyperfine coupling tensor between the Si nucleus and the i-th U site of the first-nearest-neighbor, and $\boldsymbol{m}_i^{(1)}$ denotes the ordered moment at the i-th U site. The second term is the same for the second-nearest-neighbor site. The hyperfine coupling tensor of the sites (1), $A_i^{(1)}$, is expressed from the consideration of symmetry as follows:

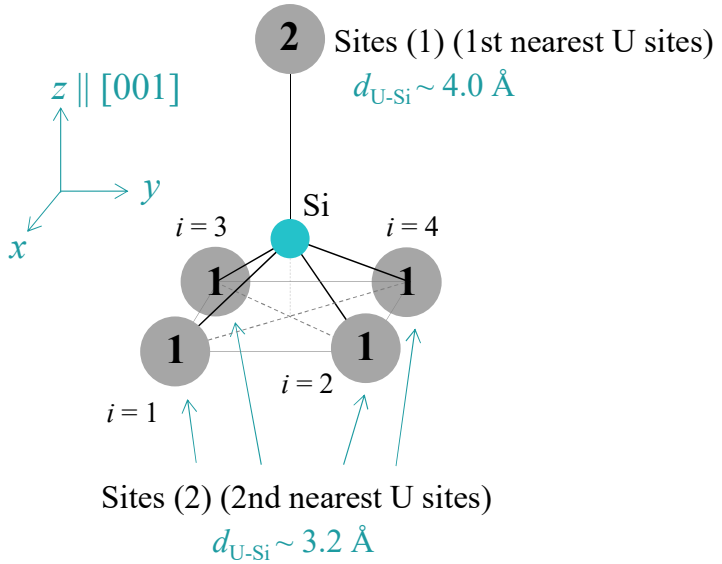

FIGURE A.1: Schematic view of a Si site and its neighboring U sites in UAu_2Si_2.

$$A_1^{(1)} = \begin{bmatrix} A_a^{(1)} & A_{ab}^{(1)} & A_{ac}^{(1)} \\ A_{ab}^{(1)} & A_a^{(1)} & A_{ac}^{(1)} \\ A_{ca}^{(1)} & A_{ca}^{(1)} & A_c^{(1)} \end{bmatrix}, \; A_2^{(1)} = \begin{bmatrix} A_a^{(1)} & -A_{ab}^{(1)} & -A_{ac}^{(1)} \\ -A_{ab}^{(1)} & A_a^{(1)} & A_{ac}^{(1)} \\ -A_{ca}^{(1)} & A_{ca}^{(1)} & A_c^{(1)} \end{bmatrix},$$
$$A_3^{(1)} = \begin{bmatrix} A_a^{(1)} & -A_{ab}^{(1)} & A_{ac}^{(1)} \\ -A_{ab}^{(1)} & A_a^{(1)} & -A_{ac}^{(1)} \\ A_{ca}^{(1)} & -A_{ca}^{(1)} & A_c^{(1)} \end{bmatrix}, \; A_4^{(1)} = \begin{bmatrix} A_a^{(1)} & A_{ab}^{(1)} & -A_{ac}^{(1)} \\ A_{ab}^{(1)} & A_a^{(1)} & -A_{ac}^{(1)} \\ -A_{ca}^{(1)} & -A_{ca}^{(1)} & A_c^{(1)} \end{bmatrix}. \tag{A.3}$$

$A^{(2)}$ has only diagonal components, since the U site (2) is located on the line extended along the c-axis from the Si site. Thus,

$$A^{(2)} = \begin{bmatrix} A_a^{(2)} & 0 & 0 \\ 0 & A_a^{(2)} & 0 \\ 0 & 0 & A_c^{(2)} \end{bmatrix}. \tag{A.4}$$

In the paramagnetic state, the magnetic moments are uniform at each U sites, namely, $\boldsymbol{m}_i^{(1)} = \boldsymbol{m}^{(2)} \equiv \boldsymbol{m}$. Therefore, we obtain

$$\boldsymbol{H}_{\rm hf} = 4\begin{bmatrix} A_a^{(1)} & 0 & 0 \\ 0 & A_a^{(1)} & 0 \\ 0 & 0 & A_c^{(1)} \end{bmatrix}\boldsymbol{m} + \begin{bmatrix} A_a^{(2)} & 0 & 0 \\ 0 & A_a^{(2)} & 0 \\ 0 & 0 & A_c^{(2)} \end{bmatrix}\boldsymbol{m}. \tag{A.5}$$

When the external field is applied along the c-axis, $\boldsymbol{m} = (0, 0, m)$, then

$$\boldsymbol{H}_{\rm hf} = 4m\begin{bmatrix} 0 \\ 0 \\ A_c^{(1)} \end{bmatrix} + m\begin{bmatrix} 0 \\ 0 \\ A_c^{(2)} \end{bmatrix} = m\begin{bmatrix} 0 \\ 0 \\ 4A_c^{(1)} + A_c^{(2)} \end{bmatrix}. \tag{A.6}$$

Here, the hyperfine field has only the c-component. From the $K - \chi$ plot, we can use the experimentally obtained value of $\sim$ 6.9 kOe/$\mu_{\rm B}$for the diagonal component, and thus obtain

$$4A_c^{(1)} + A_c^{(2)} = 6.9({\rm kOe}/\mu_{\rm B}). \tag{A.7}$$

A.2 Hyperfine coupling fields in the ordered states

In the ordered state, the similar examination can be taken. Here we consider some cases of possible spin structures.

Case (i): AFM with q = (2/3, 0, 0), and $\boldsymbol{m} = \pm$(0, 0, m)

There are three magnetically nonequivalent Si sites as shown in Fig. A.2: At the Si site 1,

$$\boldsymbol{m}_1^{(1)} = \boldsymbol{m}_2^{(1)} = \boldsymbol{m}_3^{(1)} = \boldsymbol{m}_4^{(1)} = -\boldsymbol{m}^{(2)} = \boldsymbol{m} = (0, 0, m); \tag{A.8}$$

therefore,

$$\boldsymbol{H}_{\rm int}^{\rm site1} = (A_1^{(1)} + A_2^{(1)} + A_3^{(1)} + A_4^{(1)} - A^{(2)})\boldsymbol{m} = m\begin{bmatrix} 0 \\ 0 \\ 4A_c^{(1)} - A_c^{(2)} \end{bmatrix}. \tag{A.9}$$

For the site 2,

$$\boldsymbol{m}_1^{(1)} = -\boldsymbol{m}_2^{(1)} = \boldsymbol{m}_3^{(1)} = -\boldsymbol{m}_4^{(1)} = \boldsymbol{m}^{(2)} = \boldsymbol{m} = (0, 0, m). \tag{A.10}$$

In the same manner as the site 1, we obtain

$$\boldsymbol{H}_{\rm int}^{\rm site2} = (A_1^{(1)} - A_2^{(1)} + A_3^{(1)} - A_4^{(1)} + A^{(2)})\boldsymbol{m} = m\begin{bmatrix} 4A_{ac}^{(1)} \\ 0 \\ A_c^{(2)} \end{bmatrix}. \tag{A.11}$$

Since the site 3 is the mirror reflection of the site 2 with respect to the ac-plane, the a-component internal field changes its sign;

$$\boldsymbol{H}_{\rm int}^{\rm site3} = (-A_1^{(1)} + A_2^{(1)} - A_3^{(1)} + A_4^{(1)} + A^{(2)})\boldsymbol{m} = m \begin{bmatrix} -4A_{ac}^{(1)} \\ 0 \\ A_c^{(2)} \end{bmatrix}. \tag{A.12}$$

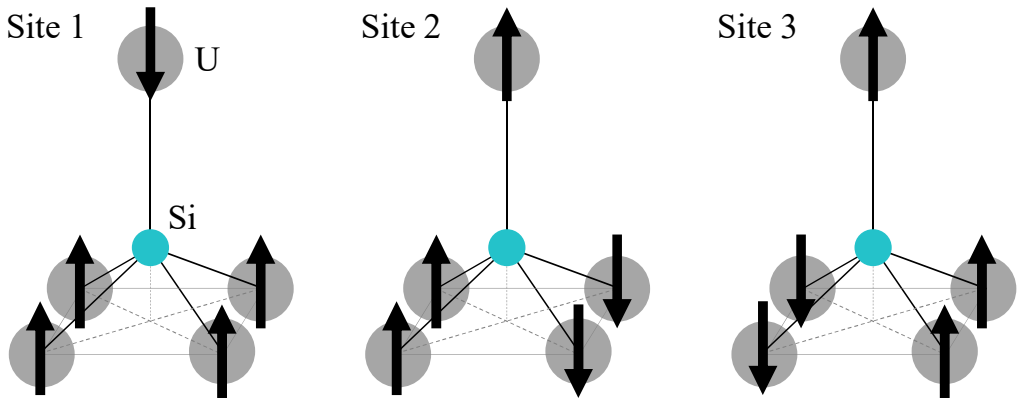

FIGURE A.2: Schematic view of spin configurations around three magnetically-nonequivalent Si sites in the magnetic structure of $\boldsymbol{q}$=(2/3, 0, 0).

The internal field of this configuration leads to the NMR spectra where two peaks with the intensity ratio of 1:2 in the lower field side of the H_0 in the external field parallel to the c-axis. This is consistent with the present experimental results. In the field perpendicular to the c-axis, the peak splitting is expected in this model. However, the present measurements were performed on the powdered sample, and the crystals are randomly oriented in the c-plane. In this condition, the spectra should be broadened in the ordered state, and this is actually observed in the present study.

Case (ii): AFM with q = (0, 0, 2/3), $m = \pm$(0, 0, m)

This case is inconsistent with the experimental results as follows. The internal field can be expressed in the same manner described above. Also, in this spin structure, there are three magnetically nonequivalent Si sites as shown in Fig. A.3. For the Si site 1, we obtain

$$\boldsymbol{m}_1^{(1)} = \boldsymbol{m}_2^{(1)} = \boldsymbol{m}_3^{(1)} = \boldsymbol{m}_4^{(1)} = \boldsymbol{m}^{(2)} = \boldsymbol{m} = (0, 0, m), \tag{A.13}$$

and

$$\boldsymbol{H}_{\rm int}^{\rm site1} = m \begin{bmatrix} 0 \\ 0 \\ 4A_c^{(1)} + A_c^{(2)} \end{bmatrix}. \tag{A.14}$$

For the site 2,

$$\boldsymbol{m}_1^{(1)} = \boldsymbol{m}_2^{(1)} = \boldsymbol{m}_3^{(1)} = \boldsymbol{m}_4^{(1)} = -\boldsymbol{m}^{(2)} = \boldsymbol{m} = (0, 0, m), \tag{A.15}$$

and

$$\boldsymbol{H}_{\rm int}^{\rm site2} = m \begin{bmatrix} & 0 & \\ & 0 & \\ 4A_c^{(1)} & - & A_c^{(2)} \end{bmatrix}. \tag{A.16}$$

For the site 3,

$$-\boldsymbol{m}_1^{(1)} = -\boldsymbol{m}_2^{(1)} = -\boldsymbol{m}_3^{(1)} = -\boldsymbol{m}_4^{(1)} = \boldsymbol{m}^{(2)} = \boldsymbol{m} = (0, 0, m), \tag{A.17}$$

and

$$\boldsymbol{H}_{\rm int}^{\rm site3} = m \begin{bmatrix} & 0 & \\ & 0 & \\ -4A_c^{(1)} & + & A_c^{(2)} \end{bmatrix}. \tag{A.18}$$

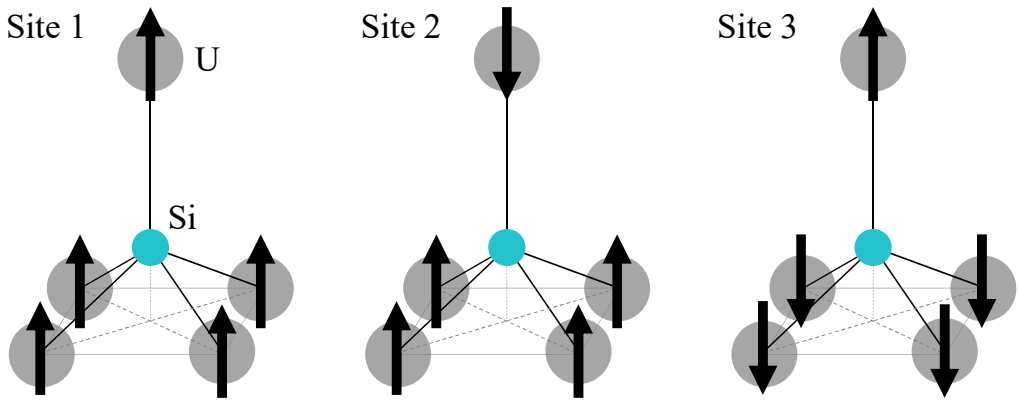

FIGURE A.3: Schematic view of spin configurations around three magnetically-nonequivalent Si sites in the magnetic structure of $\boldsymbol{q}$=(0, 0, 2/3).

These internal fields lead to the NMR spectra with three separated peaks with equal size, two of which are in the lower field side and one is in the higher side of the H_0, when the external field is applied in parallel to the c-axis. This is the first inconsistent point with the experimental results. The second one is that the expected spectra do not show any line splitting in the external field perpendicular to the c-axis. This fact cannot explain the large broadening of the obtained spectra.

Other typical structures have also been examined, but no other structure explains the experimental results more successfully than that of the case (i). For example, we tested following cases:

(iii) $\boldsymbol{q}$ = (0, 0, 1), $\boldsymbol{m} \parallel c$; type-I AFM structure, which is the most typical magnetic structure in the UT_2Si$_2$ family.

(iv) $\boldsymbol{q}$ = (1/2, 1/2, 0), $\boldsymbol{m} \parallel$ [110]; several CeT_2Si$_2$ compounds employ this structure, in which the ordered moments are lying in the c-plane.

(v) $\boldsymbol{q}$ = (2/3, 2/3, 0), $\boldsymbol{m} \parallel c$; another candidate of the up-up-down structure.

None of these structures gives the NMR spectra in $H_{\parallel}$ consistent with the observed one; in the case (iii), the NMR spectrum of which the line splits into two around H_0 with the intensity ratio of 1 : 1 is expected. In the case (iv), the resonance peak in the expected NMR spectrum does not split, with a single peak at H_0 because the c-component of the hyperfine field is canceled out. In the case (v), two resonance peaks are expected below H_0. This is consistent with the experimental result. However, the expected intensity ratio is not $I_{\rm small} : I_{\rm large}$ = 1 : 2 as observed, but 2 : 1. Consequently, we concluded that the most possible magnetic structure in UAu_2Si_2 is that of the case (i); $i.e.$, the uncompensated AFM structure with $\boldsymbol{q}$ = (2/3, 0, 0).

A.3 Semiquantitative estimation of the ordered moments

In this section, we try to estimate the ordered moments, assuming the magnetic structure of the case (i). We proceed the model approximation in the following manner; first only the transferred hyperfine fields due to local spins are taken into account as we have already presented in the former section. Second, the temperature-independent contribution to the hyperfine fields is added. In the end of the procedure, the long-range dipolar fields will be considered.

A.3.1 The local spin model

In the ordered state, we have the ordered magnetic moment $m_{\rm ord}$ pointing to the c axis:

$$\boldsymbol{m}_{\rm ord} = (0, 0, m_{\rm ord}).$$

Here, we assume that the internal field that the Si nuclei spins feel comes only from the hyperfine contribution of the local spins, $\boldsymbol{H}_{\rm hf}^{S}$; namely,

$$\boldsymbol{H}_{\rm int} = \boldsymbol{H}_{\rm hf}^{S},$$

which are described at each Si site as follows:

$$\boldsymbol{H}_{\rm int}^{\rm site1} = m_{\rm ord} \begin{bmatrix} 0 \\ 0 \\ 4A_c^{(1)} - A_c^{(2)} \end{bmatrix},$$

$$\boldsymbol{H}_{\rm int}^{\rm site2} = m_{\rm ord} \begin{bmatrix} 4A_{ac}^{(1)} \\ 0 \\ A_c^{(2)} \end{bmatrix},$$

$$\boldsymbol{H}_{\rm int}^{\rm site3} = m_{\rm ord} \begin{bmatrix} -4A_{ac}^{(1)} \\ 0 \\ A_c^{(2)} \end{bmatrix}.$$

Here, we discuss the case of $\boldsymbol{H}_{\rm ext} \| \boldsymbol{c}$. The observed small peak is from the resonance at the site 1, where the nuclear spins feel a higher internal field of $H_{{\rm int},c} \sim 6.2$ kOe, and the large peak is from the site 2 and site 3 with the lower internal field of $H_{{\rm int},c} \sim 2.2$ kOe. Thus, we obtain the relations:

$$H_{\rm int}^{c}({\rm site1}) = m_{\rm ord}(4A_c^{(1)} - A_c^{(2)}) = 6.2({\rm kOe}), \tag{A.19}$$

and

$$H_{\rm int}^{c}({\rm site2,3}) = m_{\rm ord}A_c^{(2)} = 2.2({\rm kOe}). \tag{A.20}$$

These two equations give

$$\begin{aligned} 4m_{\rm ord}A_c^{(1)} &= 6.2 + 2.2 = 8.4\ ({\rm kOe}), \\ \therefore m_{\rm ord}A_c^{(1)} &= 2.1({\rm kOe}). \end{aligned} \tag{A.21}$$

On the other hand, in the paramagnetic state,

$$\boldsymbol{H}_{\rm int} = \boldsymbol{m}_{\rm p} \begin{bmatrix} 0 \\ 0 \\ 4A_c^{(1)} + A_c^{(2)} \end{bmatrix}. \tag{A.22}$$

Since the $K - \chi$ plot gives the hyperfine coupling constant as ~ 6.9 kOe/$\mu_{\rm B}$, we can obtain another relation:

$$4A_c^{(1)} + A_c^{(2)} = 6.9\ ({\rm kOe}/\mu_{\rm B}). \tag{A.23}$$

From the Eqs. (A.19), (A.20), and (A.23),

$$\begin{aligned} m_{\rm ord}(4A_c^{(1)} + A_c^{(2)}) &= 4 \times 2.1 + 2.2 \sim 10.6 \\ &= m_{\rm ord} \times 6.9 \end{aligned} \tag{A.24}$$

Therefore, we finally obtain the parameters as follows:

$$\begin{aligned} m_{\rm ord} &\sim 1.536 \sim 1.5\ (\mu_{\rm B}), \\ A_c^{(1)} &\sim 1.432 \sim 1.4\ ({\rm kOe}/\mu_{\rm B}), \\ A_c^{(2)} &\sim 1.367 \sim 1.4\ ({\rm kOe}/\mu_{\rm B}), \end{aligned} \tag{A.25}$$

A.3.2 Inclusion of the T-independent contribution

Here, we assume that the internal field is composed of the temperature-dependent contribution from the local spins, $\boldsymbol{H}_{\rm hf}^{S}$, and the temperature-independent contribution, $\boldsymbol{H}_{\rm hf}^{\rm orb}$;

$$\boldsymbol{H}_{\rm int} = \boldsymbol{H}_{\rm hf}^{S} + \boldsymbol{H}_{\rm hf}^{\rm orb}. \tag{A.26}$$

The latter is due to orbital contribution to the hyperfine coupling, paramagnetic on-site contribution by the itinerant electrons, and contribution of Van-Vleck paramagnetism, and so on. Assuming that the hyperfine coupling tensor $A_{\rm hf}^{\rm orb}$ gives the $\boldsymbol{H}_{\rm hf}^{\rm orb}$, and that it has only the diagonal components:

$$A_{\rm hf}^{\rm orb} = \begin{bmatrix} A_a^{\rm orb} & 0 & 0 \\ 0 & A_a^{\rm orb} & 0 \\ 0 & 0 & A_c^{\rm orb} \end{bmatrix}. \tag{A.27}$$

Considering $\boldsymbol{H}_{\rm ext} \parallel \boldsymbol{m}_{\rm orb} \parallel c$, we get

$$\boldsymbol{H}_{\rm int}^{\rm orb} = \begin{bmatrix} 0 \\ 0 \\ A_c^{\rm orb} m_{\rm orb} \end{bmatrix}. \tag{A.28}$$

Hence the internal fields at each Si sites are described as

$$\boldsymbol{H}_{\rm int}^{\rm site1} = m_{\rm ord} \begin{bmatrix} 0 \\ 0 \\ 4A_c^{(1)} - A_c^{(2)} \end{bmatrix} + m_{\rm vv} \begin{bmatrix} 0 \\ 0 \\ A_c^{\rm orb} \end{bmatrix}, \tag{A.29}$$

$$\boldsymbol{H}_{\rm int}^{\rm site2} = m_{\rm ord} \begin{bmatrix} 4A_{ac}^{(1)} \\ 0 \\ A_c^{(2)} \end{bmatrix} + m_{\rm vv} \begin{bmatrix} 0 \\ 0 \\ A_c^{\rm orb} \end{bmatrix}, \tag{A.30}$$

and

$$\boldsymbol{H}_{\rm int}^{\rm site3} = m_{\rm ord} \begin{bmatrix} -4A_{ac}^{(1)} \\ 0 \\ A_c^{(2)} \end{bmatrix} + m_{\rm vv} \begin{bmatrix} 0 \\ 0 \\ A_c^{\rm orb} \end{bmatrix}, \tag{A.31}$$

where $m_{\rm orb}$ is rewritten as $m_{\rm vv}$, because $m_{\rm ord}$ and $m_{\rm orb}$ are confusing.

When we compare these with the experimental results for $\mathbf{H}_{\rm ext} \parallel \mathbf{c}$, we get

$$H_{\rm int}^c({\rm site1}) = m_{\rm ord}(4A_c^{(1)} - A_c^{(2)}) + A_c^{\rm orb} m_{\rm vv} = 6.1\ ({\rm kOe}), \tag{A.32}$$

and

$$H_{\rm int}^c({\rm site2,3}) = m_{\rm ord} A_c^{(2)} + A_c^{\rm orb} m_{\rm vv} = 2.2\ ({\rm kOe}), \tag{A.33}$$

with five unknown parameters. To solve these, we estimate $A_c^{\rm orb}$ and $m_{\rm vv}$ from the intercept of the K-χ plot and the experimental results of magnetization, respectively.

First we discuss $m_{\rm vv}$. Figure A.4 shows the magnetization along the c-axis measured on the single-crystalline sample at 4 K. In order to extract a paramagnetic com-

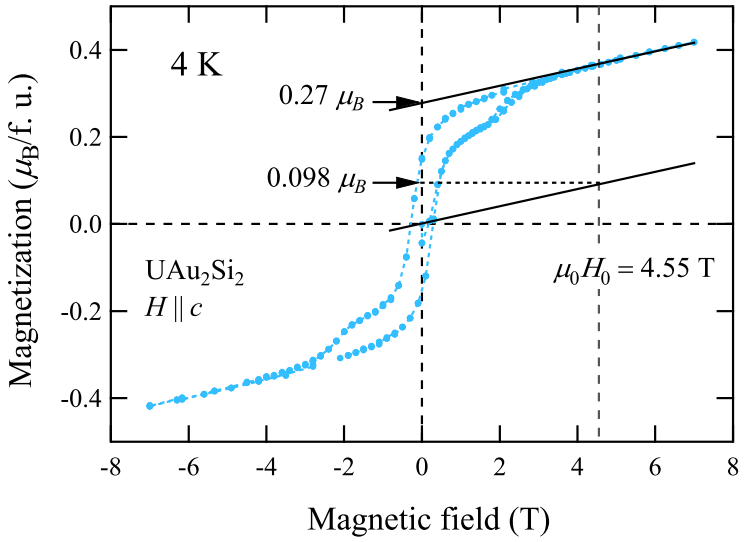

FIGURE A.4: Magnetization curve along the c-axis measured on the single crystalline-sample of UAu_2Si_2 at 4 K. The solid line on the data is an extrapolating line and by shifting it, the linear component is displayed as the another solid line. The broken line shows H_0 = 4.55 T.

ponent, we assume that the measured magnetization curve is a sum of "the FM component which saturates by the field of ∼2 T" and "the paramagnetic component linear to the applied field". Then, by extrapolating the line drawn in the higher field range above 2 T to zero field, the saturating FM component is estimated to be $\sim 0.27\ \mu_{\rm B}$per U atom. The magnitude of the paramagnetic component is estimated from the tangent of this line to be about 0.099 $\mu_{\rm B}$/U at 4.55 T. We use this value as $m_{\rm vv}$ for the discussion.

Next we estimate $A_c^{\rm orb}$. The hyperfine coupling constant estimated from the slope of the$K$-χ plot does not contain the temperature-independent contribution. In general, the Knight shift is expressed by the sum of T-dependent spin contribution, the T-independent orbital contribution, and the diamagnetic field contribution.

$$K = A^S \chi^S(T) + A^{\rm orb}\chi^{\rm orb} + A^{\rm dia}\chi^{\rm dia}. \tag{A.34}$$

We can separate the T-dependent and T-independent contributions by using the linear part of the K-χ plot as follows:

$$(\text{Slope}) = A^S.$$

$$(\text{ Intersect of the } \textit{“K”-axis}) = (A^{\rm orb} - A^S)\chi^{\rm orb} + (A^{\rm dia} - A^S)\chi^{\rm dia}.$$

Here, the diamagnetic contribution is assumed to be negligible, and the experimental value of the intersect of 0.550 (%) is applied; then, we get

$$(A_c^{\rm orb} - A^S)\chi^{\rm orb} = 0.550. \tag{A.35}$$

Then by using the value of $m_{\rm vv} = 0.099$ ($\mu_{\rm B}$/U), we get

$$\chi^{\rm orb} = m_{\rm vv}/45500 = 0.099/45500 \sim 2.16 \times 10^{-6}\ (\mu_B/\text{Oe/f.u.}). \tag{A.36}$$

Combining this with the spin contribution of $A_c^S = 6.9$ (kOe/μ_B),

$$(A_c^{\rm orb} - 6900) \times 2.16 \times 10^{-6} = 0.550 \times 10^{-2}, \tag{A.37}$$

and thus

$$A_c^{\rm orb} \sim 9.45 \ ({\rm kOe}/\mu_B). \tag{A.38}$$

Hence, the c-components of the internal field at each Si site are expressed as

$$\begin{aligned} H_{{\rm int},c}^{\rm site1} &= m_{\rm ord}(4A_c^{(1)} - A_c^{(2)}) + A_c^{\rm orb} m_{\rm vv} = 6.2 \ ({\rm kOe}), \\ \therefore m_{\rm ord}(4A_c^{(1)} - A_c^{(2)}) &= 6.2 - 9.45 \times 0.0985 \sim 5.27{\rm kOe}; \end{aligned} \tag{A.39}$$

$$\begin{aligned} H_{{\rm int},c}^{\rm site2,3} &= m_{\rm ord} A_c^{(2)} + A_c^{\rm orb} m_{\rm vv} = 2.2 \ ({\rm kOe}), \\ \therefore m_{\rm ord} A_c^{(2)} &= 2.2 - 9.45 \times 0.0985 \sim 1.27 \ ({\rm kOe}). \end{aligned} \tag{A.40}$$

Now the equations (A.23), (A.39) and (A.40) can be solved, yielding the parameters:

$$\begin{aligned} m_{\rm ord} &\sim 1.1 \ (\mu_B), \\ A_c^{(1)} &\sim 1.4 \ ({\rm kOe}/\mu_B), \\ A_c^{(2)} &\sim 1.1 \ ({\rm kOe}/\mu_B). \end{aligned}$$

As shown here, $m_{\rm ord}$ and the $A_c^{(2)}$ are suppressed, while $A_c^{(1)}$ is enhanced. When considering the intersite distance between a Si site and its first or second nerest neighbor U sites, this relationship in the magnitude of the hyperfine coupling constants is considered to be more practical than that in the former section.

A.3.3 Inclusion of the dipolar-field effect

Let us now add the contribution of dipolar field produced by the local ordered spins to the internal field. The $\boldsymbol{H}_{\rm int}$ here is written as

$$\boldsymbol{H}_{\rm int}^{\rm site1} = m_{\rm ord} \begin{bmatrix} 0 \\ 0 \\ 4A_c^{(1)} - A_c^{(2)} \end{bmatrix} + m_{\rm vv} \begin{bmatrix} 0 \\ 0 \\ A_c^{\rm orb} \end{bmatrix} + \begin{bmatrix} H_{1,a}^{\rm dip} \\ H_{1,b}^{\rm dip} \\ H_{1,c}^{\rm dip} \end{bmatrix}, \tag{A.41}$$

$$\boldsymbol{H}_{\rm int}^{\rm site2} = m_{\rm ord} \begin{bmatrix} 4A_{ac}^{(1)} \\ 0 \\ A_c^{(2)} \end{bmatrix} + m_{\rm vv} \begin{bmatrix} 0 \\ 0 \\ A_c^{\rm orb} \end{bmatrix} + \begin{bmatrix} H_{2,a}^{\rm dip} \\ H_{2,b}^{\rm dip} \\ H_{2,c}^{\rm dip} \end{bmatrix}, \tag{A.42}$$

$$\boldsymbol{H}_{\rm int}^{\rm site3} = m_{\rm ord} \begin{bmatrix} -4A_{ac}^{(1)} \\ 0 \\ A_c^{(2)} \end{bmatrix} + m_{\rm vv} \begin{bmatrix} 0 \\ 0 \\ A_c^{\rm orb} \end{bmatrix} + \begin{bmatrix} H_{3,a}^{\rm dip} \\ H_{3,b}^{\rm dip} \\ H_{3,c}^{\rm dip} \end{bmatrix}. \tag{A.43}$$

The dipolar field at the Si sites generated by the ordered U moments of 1 $\mu_{\rm B}$/U with the magnetic structure of $\boldsymbol{q} = (2/3, 0, 0)$ can be simulated as

$$\frac{1}{m_{\rm ord}} \begin{bmatrix} H^{\rm dip}_{1,a} \\ H^{\rm dip}_{1,b} \\ H^{\rm dip}_{1,c} \end{bmatrix} = \begin{bmatrix} 0 \\ 0 \\ -1.00 \end{bmatrix} \ ({\rm kOe}), \tag{A.44}$$

$$\frac{1}{m_{\rm ord}} \begin{bmatrix} H^{\rm dip}_{2,a} \\ H^{\rm dip}_{2,b} \\ H^{\rm dip}_{2,c} \end{bmatrix} = \begin{bmatrix} 0.909 \\ 0 \\ -0.297 \end{bmatrix} \ ({\rm kOe}), \tag{A.45}$$

$$\frac{1}{m_{\rm ord}} \begin{bmatrix} H^{\rm dip}_{3,a} \\ H^{\rm dip}_{3,b} \\ H^{\rm dip}_{3,c} \end{bmatrix} = \begin{bmatrix} -0.909 \\ 0 \\ -0.297 \end{bmatrix} \ ({\rm kOe}). \tag{A.46}$$

For this calculation, the contribution from the U sites within a radius of 20 Å from the Si site were summed up. Using these values, the c-components of $\boldsymbol{H}_{\rm int}$ at each Si site in the ordered state are written as

$$\begin{aligned} H^{\rm site1}_{{\rm int},c} &= m_{\rm ord}(4A^{(1)}_c - A^{(2)}_c - 1.00) + 0.931 = 6.2 \ ({\rm kOe}), \\ \therefore m_{\rm ord}(4A^{(1)}_c - A^{(2)}_c - 1.00) &= 5.17 \ ({\rm kOe}); \end{aligned} \tag{A.47}$$

$$\begin{aligned} H^{\rm site2,3}_{{\rm int},c} &= m_{\rm ord}(A^{(2)}_c - 0.297) + 0.931 = 2.2 \ ({\rm kOe}), \\ \therefore m_{\rm ord}(A^{(2)}_c - 0.297) &= 1.27 \ ({\rm kOe}). \end{aligned} \tag{A.48}$$

It is also necessary to consider the dipolar-field contribution in the paramagnetic state to derive the $\boldsymbol{H}_{\rm int}$. Then, calculation gives the relation:

$$\boldsymbol{H}^{\rm para}_{{\rm int},c} = m_{\rm para} \begin{bmatrix} 0 \\ 0 \\ 4A^{(1)}_c + A^{(2)}_c \end{bmatrix} + m_{\rm para} \begin{bmatrix} 0 \\ 0 \\ -0.407 \end{bmatrix} \ ({\rm kOe}). \tag{A.49}$$

The second term corresponds to the dipolar field when uniform paramagnetic moments in magnitude of $m_{\rm para}$ ($\mu_{\rm B}$) are induced at each U sites. Here again we use the value of the spin contribution to the hyperfine coupling interaction of 6.9 kOe/$\mu_{\rm B}$;

$$\begin{aligned} 4A^{(1)}_c + A^{(2)}_c - 0.407 &= 6.9 \ ({\rm kOe}), \\ \therefore 4A^{(1)}_c + A^{(2)}_c &= 7.307 \ ({\rm kOe}). \end{aligned} \tag{A.50}$$

Equations A.50 and A.50 can be solved as;

$$\begin{aligned} m_{\mathrm{ord}} &\sim 1.3665 \sim 1.4\ (\mu_{\mathrm{B}}), \\ A_c^{(1)} &\sim 1.5203 \sim 1.5\ (\mathrm{kOe}/\mu_{\mathrm{B}}), \\ A_c^{(2)} &\sim 1.2256 \sim 1.2\ (\mathrm{kOe}/\mu_{\mathrm{B}}). \end{aligned}$$

The ordered moment is not affected very much by the treatment of the dipolar fields while the difference between the hyperfine coupling constants of the first and second nearest neighbor is enlarged.

This magnitude of the magnetically ordered moment gives the FM saturation component of the magnetization of $\sim 0.47\ (\mu_{\mathrm{B}}/\mathrm{f.u.}) = 1.4/3\ (\mu_{\mathrm{B}})$, which is larger than the actually measured value of 0.26 ($\mu_{\mathrm{B}}/\mathrm{f.u.}$). Nevertheless, we may safely state that this simple local-spin model provides a fairly good semiquantitative description of the magnetic properties of this compound.

References

[1] N. T. Huy et al. "Superconductivity on the border of weak itinerant ferromagnetism in UCoGe". In: *Phys. Rev. Lett.* 99 (2007), p. 067007.

[2] D. Aoki et al. "Coexistence of superconductivity and ferromagnetism in URhGe". In: *Nature* 43 (2001), p. 613.

[3] A. Huxley et al. "UGe_2: A ferromagnetic spin-triplet superconductor". In: *Phys. Rev. B* 63 (2001), p. 144519.

[4] T. D. Matsuka et al. "Single crystal growth and structural and magnetic properties of the uranium ternary intermetallic compound UCr_2Si_2". In: *J. Phys. Soc. Jpn.* 72 (2003), p. 122.

[5] A. Szytula et al. "Neutron diffraction study of UT_2X_2 (T = Mn, Fe, X = Si, Ge) intermetallic systems". In: *J. Phys. Chem. Solids* 49 (1988), p. 1113.

[6] L. Chelmicki, J. Leciefewicz, and A. Zygmunt. "Magnetic properties of UT_2Si_2 and UT_2Ge_2 (T = Co, Ni, Cu) intermetallic systems". In: *J. Phys. Chem. Solids* 46 (1985), p. 579.

[7] H. Lin et al. "Magnetic structure of UNi_2Ni_2". In: *Phys. Rev. B* 43 (1991), p. 13232.

[8] T. D. Matsuda et al. "Electrical and Magnetic Properties of a Single Crystal UCu_2Si_2". In: *J. Phys. Soc. Jpn.* 74 (2005), p. 1552.

[9] F. Honda et al. "Long-period, longitudinal spin density modulation in an itinerant 5f magnetic compound UCu_2Si_2". In: *J. Phys. Cond. Matt.* 18 (2006), p. 479.

[10] T. T. M. Palstra et al. "Superconducting and magnetic transitions in the heavy-fermion system URu_2Si_2". In: *Phys. Rev. Lett.* 55 (1985), p. 2727.

[11] M. B. Maple et al. "Partially gapped Fermi surface in the heavy-electron superconductor URu_2Si_2". In: *Phys. Rev. Lett.* 56 (1986), p. 185.

[12] W. Schlabitz et al. "Superconductivity and magnetic order in a strongly interacting fermi-system: URu_2Si_2". In: *Z. Phys. B Cond. Matt.* 62 (1986), p. 171.

[13] H. Ptasiewicz-Bak, J. Leciejewicz, and A. Zygmunt. "Neutron diffraction study of magnetic ordering in UPd_2Si_2, UPd_2Ge_2, URh_2Si_2 and URh_2Ge_2". In: *J. Phys. F: Metal Phys.* 11 (1981), p. 225.

[14] T. T. M. Palstra et al. "Magnetic properties of the ternary compounds CeT_2Si_2 and UT_2Si_2". In: *J. Magn. Magn. Mater.* 54-57 (1986), p. 435.

[15] T. Honma et al. "Incommensurate-commensurate magnetic phase transitions of the Ising-5f system UPd_2Si_2: the H-T phase diagram and mean-field analyses". In: *J. Phys. Soc. Jpn.* 67 (1998), p. 1017.

[16] A. J. Dirkmaat et al. "Magnetic and transport properties of various UT_2Ge_2 (T = 3d element) intermetallic compounds". In: *J. Magn. Magn. Mater.* 84 (1990), p. 143.

[17] A. Verniére et al. "Magnetic structure and physical properties of the heavy fermion UIr_2Si_2". In: *J. Magn. Magn. Mater.* 153 (1996), p. 55.

[18] R. A. Steeman et al. "Hybridisation effects in UPt_2Si_2". In: *J. Phys. Cond. Matt.* 2 (1990), p. 4059.

[19] S. Süllow et al. "Electronic localization and two-dimensional metallic state in UPt_2Si_2". In: *J. Phys. Soc. Jpn.* 77 (2008), p. 024708.

[20] K. J. Lin et al. "Annealing effects on the physical properties of UAu_2Si_2". In: *Solid State Commun.* 103 (1997), p. 185.

[21] W. Schlabitz et al. Poster presented at the Fourth International Conference on Valence Fluctuations, ICVF, Cologne. 1984.

[22] G. Motoyama, T. Nishioka, and N. K. Sato. "Phase transition between hidden and antiferromagnetic order in URu_2Si_2". In: *Phys. Rev. Lett.* 90 (2003), p. 166402.

[23] H. Amitsuka et al. "Pressure-temperature phase diagram of the heavy-electron superconductor URu_2Si_2". In: *J. Magn. Magn. Mater.* 310 (2007), p. 214.

[24] Y. Kasahara et al. "Exotic superconducting properties in the electron-hole-compensated heavy-fermion "semimetal" URu_2Si_2". In: *Phys. Rev. Lett.* 99 (2007), p. 116402.

[25] G. Li et al. "Bulk evidence for a time-reversal symmetry broken superconducting staate in URu_2Si_2". In: *Phys. Rev. B* 88 (2013), p. 134517.

[26] L. Rebelsky et al. "Magnetic and structural phase transition in UAu_2Si_2". In: *J. Appl. Phys.* 69 (1991), p. 4810.

[27] C. Broholm et al. "Magnetic Excitations and Ordering in the Heavy-Electron Superconductor URu_2Si_2". In: *Phys. Rev. Lett.* 58 (1987), p. 1467.

[28] M. J. Bull et al. "Search for novel order in URu_2Si_2 by neutron scattering". In: *Acta Physica Polonica B* 34 (2003), p. 1265.

[29] C. R. Wiebe et al. "Search for hidden orbital currents and observation of an activated ring of magnetic scattering in the heavy fermion superconductor URu_2Si_2". In: *Phys. Rev. B* 69 (2004), p. 132418.

[30] Y. Ikeda et al. "Search for hidden order parameter of URu_2Si_2 by neutron scattering experiment under uniaxial stress". In: *J. Phys: Conf. Ser.* 200 (2010), p. 012065.

[31] E. D. Isaacs et al. "X-ray magnetic scattering in antiferromagnetic URu_2Si_2". In: *Phys. Rev. Lett.* 25 (1990), p. 3185.

[32] N. Kernavanois et al. "Investigation of the crystal structure of URu_2Si_2 by high-resolution X-ray diffraction". In: *Physica B* 259-261 (1999), p. 648.

[33] H. Amitsuka et al. "Resonant X-ray scattering study of hidden order in URu_2Si_2 using a low-stress single crystal". In: *J. Phys. Conference Series* 200 (2010), p. 012007.

[34] H. C. Walker et al. "Resonant x-ray scattering study of the URu_2Si_2 hidden-order phase". In: *Phys. Rev. B* 83 (2011), p. 193102.

[35] J. A. Mydosh and P. M. Oppeneer. "Colloquium: Hidden order, superconductivity, and magnetism: The unsolved case of URu_2Si_2". In: *Rev. Mod. Phys.* 83 (2011), p. 1301.

[36] J. A. Mydosh and P. M. Oppeneer. "Hidden order behaviour in URu_2Si_2 (A critical review of the status of hidden order in 2014)". In: *Philosophical Magazine* (2014).

[37] R. Okazaki et al. "Rotational symmetry breaking in the hidden-order phase of URu_2Si_2". In: *Science* 331 (2011), p. 439.

[38] T. Shibauchi and Y. Matsuda. "Broken symmetries in URu_2Si_2". In: *Philosophical Magazine* 94 (2014), p. 3747.

[39] S. Tonegawa et al. "Cyclotron resonance in the hidden-order phase of URu_2Si_2". In: *Phys. Rev. Lett.* 109 (2012), p. 036401.

[40] S. Tonegawa et al. "Cyclotron resonance study of quasiparticle mass and scattering rate in the hidden-order and superconducting phases of URu_2Si_2". In: *Phys. Rev. B* 88 (2013), p. 245131.

[41] S. Kambe et al. "NMR study of in-plane twofold ordering in URu_2Si_2". In: *Phys Rev. Lett.* 110 (2013), p. 246404.

[42] S. Tonegawa et al. "Direct observation of lattice symmetry breaking at the hidden-order transition in URu_2Si_2". In: *Nature Commn.* (2015), DOI: 10.1038/ncomms5188.

[43] S. C. Riggs et al. "Evidence for a nematic component to the hidden order parameter in URu_2Si_2 from differential elastoresistance measurements". In: *arXiv* (2014), p. 1405.7402v1.

[44] B. Fak et al. "Influence of sample quality on the magnetic properties of URu_2Si_2". In: *J. Magn. Magn. Mater.* 154 (1996), p. 339.

[45] T. D. Matsuda et al. "Details of sample dependence and transport properties of URu_2Si_2". In: *J. Phys. Soc. Jpn.* 80 (2011), p. 114710.

[46] T. D. Matsuda. Private communication. 2015.

[47] A. de Visser et al. "Thermal expansion and specific heat of monocrystalline URu_2Si_2". In: *Phys. Rev. B* 34 (1986), p. 8168.

[48] K. Kuwahara et al. "Lattice instability and elastic response in the heavy electron system URu_2Si_2". In: *J. Phys. Soc. Jpn.* 66 (1997), p. 3251.

[49] P. Thalmeier et al. "Elastic constant anomalies and the superconducting B-T phase diagrams of UPt_3 and URu_2Si_2". In: *Physica C* 175 (1991), p. 61.

[50] B. Luthi et al. "Strain-spin density wave coupling in heavy fermion compounds". In: *Phys. Lett. A* 175 (1993), p. 237.

[51] B. Wolf et al. "Elastic properties of the heavy fermion superconductor URu_2Si_2". In: *J. Low. Temp. Phys.* 94 (1994), p. 307.

[52] T. Yanagisawa et al. "Elastic constants of $U(Ru_{1-x}Rh_x)_2Si_2$". In: *J. Phys.: Conf. Ser.* 200 (2010), p. 012236.

[53] T. Yanagisawa et al. "Γ_3-type lattice instablitity and the hidden order of URu_2Si_2". In: *J. Phys. Soc. Jpn.* 82 (2013), p. 013601.

[54] T. Yanagisawa. "Ultrasonic study of hidden order and heavy fermion state in URu_2Si_2 with hydrostatic pressure Rh-doping and high magnetic fields". In: *Phil. Mag.* (2014).

[55] T. Inami et al. "Large ferroquadrupole moment induced in the octupole-ordered $Ce_{0.7}La_{0.3}B_6$ revealed by high resolution x-ray diffraction". In: *Phys. Rev. B* 90 (2014), p. 041108.

[56] P. G. Niklowitz et al. "New angles on the border of antiferromagnetism in NiS_2 and URu_2Si_2". In: *Physica B* 404 (2009), p. 2955.

[57] P. G. Niklowitz et al. "Parastic small-moment antiferromagnetism and nonlinear coupling of hidden order and antiferromagnetism in URu_2Si_2 observed by larmor diffraction". In: *Phys. Rev. Lett.* 104 (2010), p. 106406.

[58] M. Yokoyama et al. "Nonequilibrium andtigerromagnetic state in the heavy electron compound URu_2Si_2". In: *Acta Phys. Pol.* 34 (2003), p. 1067.

[59] M. Yokoyama et al. "Competition between hidden order and antiferromagnetism in URu_2Si_2 under uniaxial stress studied by neutron scattering". In: *Phys. Rev. B* 72 (2005), p. 214419.

[60] F. Bourdarot et al. "Magnetic properties of URu_2Si_2 under uniaxial stress by neutron scattering". In: *Phys. Rev. B* 84 (2011), p. 188430.

[61] K. Matsuda et al. "Spatially inhomogeneous development of antiferromagnetism in URu_2Si_2: Evidence from ^{29}Si NMR under pressure". In: *Phys. Rev. Lett.* 87 (2001), p. 087203.

[62] H. Amitsuka et al. "Inhomogeneous magnetism in URu_2Si_2 studied by muon spin relaxation under high pressure". In: *Physica B* 326 (2003), p. 418.

[63] S. Takagi et al. "Symmetry of the hidden order in URu_2Si_2 from nuclear magnetic resonance studies". In: *J. Phys. Soc. Jpn.* 81 (2012), p. 114710.

[64] Our own experimental data taken by using the same quality single crystals. 2015.

[65] P. E. Brommer. "Mangetovolume effects and Gruneisen parameters in the stoner model". In: *Physica B* 112 (1982), p. 343.

[66] A. de Visser, J. J. M. Franse, and J. Flouquet. "Magneto-volume effects in some selected heavy-fermion compounds". In: *Physica B* 161 (1989), p. 324.

[67] M. E. Fisher. "Relation between the specific heat and susceptibility of an antiferromagnet". In: *Phil. Mag.* 7 (1962), p. 1731.

[68] H. Kitaguchi, S. Nagata, and T. Watanabe. "Antiferromagnetic ordering in $Mn(NH_3)_2{\cdot}Ni(CN)_4{\cdot}2C_6H_6$". In: *J. Phys. Soc. Jpn.* 41 (1976), p. 1159.

[69] G. J. Nieuwenhuys. "Crystalline electric field effects in UPt_2Si_2 and URu_2Si_2". In: *Phys. Rev. B* 35 (1986), p. 5260.

[70] A. E. Sikkema et al. "Ising-Kondo lattice with transverse field: A possible f-moment Hamiltonian for URu_2Si_2". In: *Phys. Rev. B* 54 (1996), p. 9322.

[71] Y. Okuno and K. Miyake. "Induced-moment weak antiferromagnetism and orbital order on the itinerant-localized duality model with nested fermi surface: A possible origin of exotic magnetism in URu_2Si_2". In: *J. Phys. Soc. Jpn.* 67 (1998), p. 2469.

[72] H. Yamagami and N. Hamada. "Relativistic electronic structure and fermi surface of URu_2Si_2 in antiferromagnetic state". In: *Physica B* 284-288 (2000), p. 1295.

[73] N. Bernhoeft et al. "Fragile thermodynamic order". In: *Acta Phys. Pol. B* 34 (2003), p. 1367.

[74] Y. Miyako et al. "Magnetic properties of $U(Ru_{1-x}Rh_x)_2Si_2$ single crystals ($0 \leq x \leq 1$)". In: *J. Appl. Phys.* 70 (1991), p. 5701.

[75] P. Santini and G. Amoretti. "Crystal field model of the magnetic properties of URu_2Si_2". In: *Phys. Rev. Lett.* 73 (1994), p. 1027.

[76] H. Amitsuka and T. Sakakibara. "Single uranium-site properties of the dilute heavy electrons system $U_xTh_{(1-x)2}Si_2$ ($x \leq 0.07$)". In: *J. Phys. Soc. Jpn.* 63 (1994), p. 63.

[77] F. J. Ohkawa and H. Shimizu. "Quadrupole and dipole orders in URu_2Si_2". In: *J. Phys. Cond. Matt.* 11 (1999), p. L519.

[78] A. Tsuruta et al. "Quadrupolar order, hidden octupolar order and tiny magnetic moment in URu_2Si_2". In: *J. Phys. Soc. Jpn* 69 (2000), p. 663.

[79] H. Harima, K. Miyake, and J. Flouquet. "Why the hidden order in URu_2Si_2 is still hidden–One simple answer". In: *J. Phys. Soc. Jpn* 79 (2010), p. 033705.

[80] P. Thalmeier and T. Takimoto. "Signatures of hidden-order symmetry in torque oscillations, elastic constant anomalies, and field-induced moments in URu_2Si_2". In: *Phys. Rev. B* 83 (2011), p. 165110.

[81] A. Kiss and P. Fazekas. "Group theory and octupolar order in URu_2Si_2". In: *Phys. Rev. B* 71 (2005), p. 054415.

[82] K. Hanzawa and N. Watanabe. "Heavy-fermion behaviours in URu_2Si_2". In: *J. Phys. Cond. Mater.* 17 (2005), p. 419.

[83] F. Cricchio et al. "Itinerant magnetic multipole moments of rank five as the hidden order in URu_2Si_2". In: *Phys. Rev. Lett.* 103 (2009), p. 107202.

[84] H. Kusunose and H. Harima. "On the hidden order in URu_2Si_2–antiferro hexadecapoly order and its consequences". In: *J. Phys. Soc. Jpn.* 80 (2011), p. 084702.

[85] M. Saran and S. P. McAlister. "Magnetic ordering in the ternary intermetallic compound UAu_2Si_2". In: *J. Magn. Magn. Mater.* 75 (1988), p. 345.

[86] M. S. Torikachvili et al. "Magnetic properties of UT_2Si_2 (T = Ni, Cu and Au) compounds". In: *J. Magn. Magn. Mater.* 104-107 (1992), p. 69.

[87] S. S. Saxena et al. "Superconductivity on the border of itinerant-electron ferromagnetism in UGe_2". In: *Nature* 406 (2000), p. 587.

[88] T. Ohta et al. "Microscopic coexistence of ferromagnetism and superconductivity in single-cystal UCoGe". In: *J. Phys. Soc. Jpn.* 79 (2010), p. 023707.

[89] K. Kadowaki and S. B. Woods. "Universal relationship of the resistivity and specific heat in heavy-fermion compounds". In: *Solid State Comm.* 58 (1986), p. 507.

[90] Y. Kohori, K. Matsuda, and T. Hohara. "^{29}Si NMR study of antiferromagnetic superconductor URu_2Si_2". In: *J. Phys. Soc. Jpn.* 65 (1996), p. 1083.

[91] Y. Kawasaki et al. "Si-NMR study of antiferromagnetic heavy-fermion compounds $CePd_2Si_2$ and $CeRh_2Si_2$". In: *Phys. Rev. B* 58 (1998), p. 8634.

[92] K. Kuwahara et al. "Magnetic structure of phase II in $U(Ru_{0.96}Rh_{0.04})_2Si_2$ determined by neutron diffraction under pulsed high magnetic fields". In: *Phys. Rev. Lett.* 110 (2013), p. 216406.

[93] J.-G. Park et al. "Thermal hysteresis in magnetization of single crystal URu_2Si_2". In: *J. Magn. Magn. Matter.* 177-181 (1998), p. 455.

[94] Y. B. Ning et al. "Magnetic and transport properties of UNi_2Ge_2". In: *Phys. Rev. B* 46 (1992), p. 8201.

[95] T. Honma et al. "Magnetic properties of single crystalline UPd_2Si_2". In: *Physica B* 186-188 (2015), p. 684.

[96] T. Endstra, G. J. Nieuwenhuys, and J. A. Mydosh. "Hybridization model for the magnetic-ordering behyavior of uranium- and cerium-based 1:2:2 intermetallic compounds". In: *Phys. Rev. B* 48 (1993), p. 9595.

[97] L. M. Sandratskii and J. Kubler. "Magnetic of UT_2Si_2 (T = Cr, Mn, Fe, Co, Ni, Cu, Ru, Rh, Pd, Os) from spin-density-functional calculations". In: *Phys. Rev. B* 50 (1994), p. 9258.

[98] S. Süllow et al. "Disorder to order transition in the magnetic and electronic properties of URh_2Ge_2". In: *Phys. Rev. B* 61 (2000), p. 8878.

[99] S. Süllow et al. "Metallic ground state and glassy transport in single crytalline URh_2Ge_2: Enhancement of disorder effects in a strongly correlated electron system". In: *Phys. Rev. Lett.* 93 (2004), p. 266602.

[100] M. Mihalik et al. "Magnetism of UCo_2Si_2 single crystal studied under applied magnetic field and hydrostatic pressure". In: *J. Phys. Soc. Jpn.* 76 (2007), p. 54.

[101] P. Svoboda et al. "Magnetic phases in UNi_2Si_2". In: *Central European Science Journals* 2 (2004), p. 397.

[102] T. Endstra et al. "Structural and magnetic properties of UCo_2Ge_2". In: *J. Appl. Phys.* 69 (1991), p. 4816.

[103] D. Niepmann and R. Pöttgen. "A single crystal study of α-$CeIr_2Si_2$, β-$CeIr_2Si_2$ and $CeIr_{1.968(5)}Si_2$". In: *Intermetallics* 9 (2001), p. 313.